Nickel(II) and copper(II) complexes of new unsymmetrically-substituted tetradentate Schiff base ligands: Spectral, structural, electrochemical and computational studies

Jonathan Cisterna, Vania Artigas, Mauricio Fuentealba, Paul Hamon, Carolina Manzur, Vincent Dorcet, Jean-René Hamon, David Carrillo

MS Ref: ICA_2016_325

Revised version

nickel(II) and copper(II) complexes of new unsymmetrically-substituted tetradentate Schiff base ligands: Spectral, structural, electrochemical and computational studies

Jonathan Cisterna[a], Vania Artigas[b], Mauricio Fuentealba[b], Paul Hamon[c], Carolina Manzur[a], Vincent Dorcet[c], Jean-René Hamon[c]*, David Carrillo[a]*

[a]Laboratorio de Química Inorgánica, Instituto de Química, Pontificia Universidad Católica de Valparaíso, Campus Curauma, Avenida Universidad 330, Valparaíso, Chile

[b]Laboratorio de Cristalografía, Instituto de Química, Pontificia Universidad Católica de Valparaíso, Campus Curauma, Avenida Universidad 330, Valparaíso, Chile

[c]Institut des Sciences Chimiques de Rennes, UMR 6226 CNRS-Université de Rennes 1, Campus de Beaulieu, 35042 Rennes Cedex, France

Corresponding authors. Phone: +33 223 23 59 58, E-mail address: jean-rene.hamon@univ-rennes1.fr (J.-R. Hamon); Phone: +56 32 227 49 14, E-mail address: david.carrillo@pucv.cl (D. Carrillo).

Abstract

The synthesis, spectroscopic and structural characterization, electrochemical properties and theoretical studies of a series of eight robust neutral Nickel(II) and Copper(II) complexes (**4**-**11**) supported by unsymmetrically-substituted N_2O_2-tetradentate Schiff base ligands are reported. The M(salophen)-type compounds are substituted by either a pair of donor (anisyl, ferrocenyl, methoxy) or acceptor (fluoro, nitro) groups, forming D-π-D and A-π-A systems, respectively. The compounds were prepared in good yields by condensation of the free amino group of the desired ONN-tridentate half-unit with the appropriate substituted salicylaldehyde in the presence of hydrated Nickel(II) or Copper(II) acetate salts. They were characterized by elemental analysis, FT-IR, UV-vis, and for diamagnetic species by multinuclear NMR spectroscopy, mass spectrometry and cyclic voltammetry. The crystal structures of one Ni(II) (**4**) and four Cu(II) complexes (**5**, **7**, **9** and **11**) revealed a four-coordinate square-planar environment for the nickel and copper metal ions, with two nitrogen and two oxygen atoms as donors. In **4**, **5**, **7** and **9**, the crystallization solvent interacts through hydrogen bonding with the phenolato oxygen atoms of the Schiff base pocket, while **11** packs as centrosymmetric dimers with an apical Cu-O short contact interaction (2.63 Å). the cyclovoltammograms of the nickel complexes present an irreversible mono-electronic Ni(II)/Ni(I) reduction wave while those of their copper counterparts exhibit a reversible or quasi-reversible one-electron Cu(II)/Cu(I) redox process. The electronic structures of the eight complexes were analyzed by DFT and TD-DFT calculations.

Keywords: Nickel; Copper; N_2O_2-ligand; Schiff base complexes; single crystal X-ray diffraction; DFT and TDDFT calculations

1. Introduction

In biological systems, transition metal ions are usually bound to a macrocycle such as a heme ring or to donor atoms of peptide chains in a distorted environment [1]. This unsymmetrical coordination of ligands around central metal ions had lead to a growing interest in the design and synthesis of transition metal complexes of unsymmetrically-substituted Schiff base ligands as synthetic models [2]. In addition, this class of compounds presents also a wide range of interesting properties, including biocidal [3], magnetic [4], nonlinear optical (NLO) [5,6], and the most commonly explored catalytic activity [7,8] among others. Compare to the straightforward preparation of their symmetrically-substituted counterparts [9], syntheses of the unsymmetrically-substituted tetradentate analogues must proceed in two steps [10,11]. The first step is monocondensation of one equivalent of an aldehyde or ketone reactant with one end of a primary diamine to give the so-called half-unit intermediates [11], which are, in a second step, allowed to react through the remaining free amino group with a different carbonyl moiety [12,13]. In some instances, half-unit intermediates can be isolated from condensation of salicylaldehyde and diamines such as 1,2-phenylenediamine or 1,2-diaminocyclohexane [13], but in the cases of 1,2-ethanediamine and 1,3-propanediamine, the half-units must be trapped as copper(II) half-unit complexes to avoid the formation of the double-condensation products [6a,15]. However, since the first report by Costes on the synthesis of the half-unit resulting from the monocondensation of 2,4-pentanedione with 1,2-ethanediamine [16], it has been extensively employed as precursor for the preparation of unsymmetrically-substituted N_2O_2-quadridentate Schiff base ligands [12,15-17]. Analogously, Ghosh *et al.* reported that monocondensation of benzoylacetone with 1,2-ethanediamine or 1,3-propanediamine under similar experimental conditions leads to the formation of the respective substituted tridentate half-units [18], that were also used to prepare unsymmetrically-substituted tetradentate Schiff base Cu(II) compounds [19] as well as trinuclear Cu(II) complexes with a μ^3-OH core [18].

Recently, we reported the X-ray crystal structure of the organometallic half-unit counterpart [20], obtained by monocondensation of ferrocenoylacetone and 1,2-ethanediamine [21]. This tridentate ferrocenyl-containing Schiff base was further functionalized by a phenolic group at the imine carbon [22], thus allowing the grafting onto a polyacrylic acid [13b]. As well, we also synthetized and structurally characterized the tridentate metalloligand formed from monocondensation of ferrocenoylacetone and 1,2-phenylenediamine, Fc-C(O)CH=C(CH3)N(H)-*o*-$C_6H_4NH_2$ (**3**, Fc = ferrocenyl = (η^5-

$C_5H_5)Fe(\eta^5\text{-}C_5H_4)))$ [23]. Those three organometallic half-units were then engaged as building blocks in the construction, upon condensation with appropriate salicylaldehydes, of a new class of unsymmetrically-substituted tetradentate Schiff base ligands and of their robust heterobimetallic nickel(II-) and copper(II)-centered complexes [13,20,24]. Such Schiff base architectures feature a delocalized planar metal-chelated macroacyclic framework that connect a ferrocene donor unit and an accepting group of the salicylidene ring, thus forming D-π-A systems exhibiting interesting second order NLO properties [13,25].

As part of our ongoing interest in this field of chemistry, we have focused on the design of two new classes of unsymmetrically-substituted D-π-D and A-π-A nickel(II) and copper(II) Schiff base complexes that could further be linked to a π-conjugated bidentate spacer to build up more expanded D-π-A systems and enhance the second-order NLO responses. We report herein on the synthesis, analytical and spectral characterization of two new half-units **1** and **2** resulting from monocondensation of 1,2-phenylenediamine with 4-methoxy and 4-fluorobenzoylacetone, respectively, and on two families of four D-π-D (**4**-**7**) and four A-π-A (**8**-**11**) metal(II)-centered macroacyclic salophen-type Schiff base complexes (see formulas on Schemes 1 and 2), formed by condensation of the free amino group of half-units **1**-**3** and salicylaldehydes bearing either donating or accepting substituents in the presence of a hydrated metal(II) acetate salt. The molecular and crystal structures of a representative example of each substitution pattern (MeO/MeO, Fc/MeO, F/F_2, F/NO_2) are also described. The X-ray structural characterisation of the octahedral $[NiCl_2(py)_4]$, formed during recrystallization of **10**, is also briefly mentioned. The electrochemical properties of the eight Schiff base complexes were studied by cyclic voltammetry. Additionally, geometry optimizations, electronic structures and theoretical assignment of the UV-Vis spectra of the complexes have been performed using DFT and TD-DFT method.

2. Experimental

2.1. Materials and general procedures

Reactions were performed under dry nitrogen atmosphere using standard Schlenk techniques. Solvents were dried and distilled according to standard procedures [26]. 5-nitrosalicylaldehyde, 3,5-difluorosalicylaldehyde, 4-methoxy-2-hydroxybenzaldehyde, 5-methoxy-2-hydroxybenzaldehyde, 1,2-phenylenediamine, nickel(II) acetate tetrahydrate, and copper(II) acetate monohydrate were purchased from Aldrich and used without further purification. 1-anisyl-1,3-butanedione [27], 1-(4-fluorophenyl)-1,3-butanedione [28] and the

organometallic tridentate "half unit" **3** [23] were synthesized according to published procedures.

2.2. Characterization

Solid-state FT-IR spectra were recorded on a Perkin-Elmer Model 1600 FT-IR spectrophotometer with KBr disks in the 4000 to 450 cm^{-1} range. Electronic spectra were obtained with a SHIMADZU UV-1800 spectrophotometer. NMR spectra were recorded at 298 K with a Bruker Avance III 400 spectrometer. All NMR spectra are reported in parts per million (ppm, δ) relative to tetramethylsilane (Me_4Si) for ^{1}H and ^{13}C NMR spectra, with the residual solvent proton and carbon resonances used as internal standards. Chemical shifts of ^{19}F NMR spectra are referenced against external $CFCl_3$. Coupling constants (*J*) are reported in Hertz (Hz), and integrations are reported as number of protons. The following abbreviations are used to describe peak patterns: s = singlet, d = doublet, t = triplet, m = multiplet, br = broad. High resolution electrospray ionization mass spectra (ESI-MS) were obtained at the Centre Regional de Mesures Physiques de l'Ouest (CRMPO, Université de Rennes 1, France) with either a WATERS Q-TOF 2, a Bruker MICROTOF-Q II or a Bruker MAXI 4G mass spectrometer. Elemental analyses were conducted on a Thermo-FINNIGAN Flash EA 1112 CHNS/O analyzer by the Microanalytical Service of the CRMPO. Cyclic voltammetry (CV) measurements were performed using a Radiometer Analytical model PGZ 100 all-in one potentiostat, using a standard three-electrode setup with a vitreous carbon working electrode, platinum wire auxiliary electrode, and Ag/Ag^{+} as the reference electrode. Dichloromethane solutions were 1.0 mM in the compound under study and 0.1 M in the supporting electrolyte *n*-$Bu_4N^{+}PF_6^{-}$ with voltage scan rate = 100 mV s^{-1}. The ferrocene/ferricenium redox couple (Cp_2Fe/Cp_2Fe^{+}) was used as internal reference for the potential measurements. Melting points were determined in evacuated capillaries on a Kofler Bristoline melting point apparatus and were not corrected.

2.3. Synthesis of (4-CH_3O-C_6H_4)C(O)CH=C(CH_3)N(H)-*o*-$C_6H_4NH_2$ (1)

A two-necked round bottom flask was charged with a stirring bar, 600 mg (3.122 mmol) of 1-anisyl-1,3-butanedione and 25 mL of dry toluene. When the solid was completely dissolved, 506 mg (4.683 mmol) of 1,2- phenylenediamine in 25 mL of dry toluene were added to the solution. Then, the flask was equipped with a Dean-Stark apparatus and the reaction mixture was refluxed for 6 h. After cooling to room temperature, the solution was reduced under vacuum to one fourth of its volume. Addition of 100 mL of petroleum ether

(35-60) caused the precipitation of a pale yellow solid. This solid was filtered off and adsorbed on a column packed with silica gel. Elution with hexane/diethyl ether mixture (1:1) produced the release of a pale yellow band which was collected. The solvent was evaporated under reduced pressure and the solid material recrystallized by slow diffusion of hexane into a dichloromethane solution of the compound, affording 565 mg (64.1% yield) of pale yellow crystals. M.p. 227-229 °C. Anal. calcd for $C_{17}H_{18}N_2O_2$ (282.34 g mol^{-1}): C, 72.32; H, 6.43; N, 9.92. Found: C, 72.09; H, 6.30; N, 9.71. HRMS-ESI$^+$ (based on $C_{17}H_{18}N_2O_2Na$ $[M^+Na]^+$) m/z calcd: 305.1266; found: 305.1264 (1 ppm). FT-IR (KBr pellet, cm^{-1}): 3450(m) ν_{asym} (NH_2), 3370(m) ν_{sym}(NH_2), 3356(w) ν(N–H), 3068(w),3040(w), 3010(w), ν(C–H aryl), 2968(w), 2940(w), 2916(w), ν(C–H alkyl), 1594(s), 1578(s) ν(C⋯O), ν(C⋯N) and/or ν(C⋯C), 1534(s) δ(NH2), 1256(s) ν(C-O), 750(s) δ(C–H). ^{1}H NMR (400 MHz, DMSO-d_6): 12.40 (s, 1 H, NH), 7.90 (d, 2 H, *4*-$C_6H_4OCH_3$), 7.01 (d, 2 H, *4*-$C_6H_4OCH_3$), 6.99 (m, 1 H, *2*-C_6H_4), 6.98 (m, 1 H, *2*-C_6H_4), 6.80 (d, 1 H, *2*-C_6H_4), 6.59 (t, 1 H, *2*-C_6H_4), 6.01 (s, 1 H, CH=C), 4.98 (s, 2 H, NH_2), 3.82 (s, 3 H, OCH_3), 1.95(s, 3 H, CH_3). ^{13}C{^{1}H}NMR (101 MHz, DMSO-d_6): 186.1 (*C*=*O*), 163.7 (CH=*C*), 161.5 (C_{quat} *4*-$C_6H_4OCH_3$), 143.9 (C_{quat} HN-C_6H_4), 132.2 (C_{quat} H_2N-C_6H_4), 128.7 (CH, *4*-$C_6H_4OCH_3$), 127.5 (CH, *2*-C_6H_4), 127.1 (CH, *2*-C_6H_4), 123.2 (C_{quat} *4*-$C_6H_4OCH_3$), 116.3 (CH, *2*-C_6H_4), 115.5 (CH, *2*-C_6H_4), 113.5 (*CH*, *4*-$C_6H_4OCH_3$), 92.5 (*C*H=C), 55.3 (OCH_3), 19.5 (CH_3).

2.4. Synthesis of (4-F-C_6H_4)C(O)CH=C(CH_3)N(H)-*o*-$C_6H_4NH_2$ (2)

The synthesis of this compound was carried out following a procedure similar to that described above for half-unit **1**, using in this case, 600 mg (3.33 mmol) of 1-(4-fluorophenyl)-1,3-butanedione and 540 mg (4.99 mmol) of 1,2- phenylenediamine, yielding 510 mg (56.6%) of a light yellow microcrystalline powder. M.p. 122-124 °C. Anal. calcd for $C_{16}H_{15}FN_2O$ (270.30 g mol^{-1}): C, 71.10; H, 5.59; N, 10.36. Found: C, 71.02; H, 5.48; N, 10.21. HRMS-ESI$^+$ (based on $C_{16}H_{15}N_2OFNa$ $[M^+Na]^+$) m/z calcd: 293.10661; found: 293.1066 (0 ppm). FT-IR (KBr pellet, cm^{-1}): 3442(m) ν_{asym} (NH_2), 3382(m) ν_{sym}(NH_2),3348(m) ν(N–H), 3066(w), 3040(w) ν(C–H), 1628(m), 1600(s), 1592(s) ν(C⋯O), ν(C⋯N) and/or ν(C⋯C), 1536(s) δ(NH_2), 1310(s) ν(C–F), 755(s) δ(C–H). ^{1}H NMR (400 MHz, DMSO-d_6): 12.43 (s, 1 H, NH), 8.00 (d, 2 H, C_6H_4F), 7.27 (t, 2 H, C_6H_4F), 7.03 (d, 1 H, *2*-C_6H_4), 7.01 (d, 1 H, *2*-C_6H_4), 6.82 (d, 1 H, *2*-C_6H_4), 6.59 (td, 1 H, *2*-C_6H_4), 6.05 (s, 1 H, *CH*=C), 5.02 (s, 2 H, NH_2), 1.97 (s, 3 H, CH_3). ^{13}C{^{1}H} NMR(101 MHz, DMSO-d_6): 185.5 (*C*=O), 164.9 (CH=*C*), 164.7 (d, $^1J_{CF}$ = 248 Hz, *C*-F), 162.5 (C_{quat}, HN-C_6H_4), 143.9 (C_{quat}, C_6H_4-NH_2), 136.1 (C_{quat}, C_6H_4-F), 129.4 (*CH*, C_6H_4-F), 127.1 (*CH*, *2*-C_6H_4), 122.9 (*CH*, *2*-C_6H_4), 116.3 (*CH*, *2*-C_6H_4), 115.2

(*CH*, *2*-C_6H_4), 115.0 (*CH*, *2*-C_6H_4), 92.7 (*C*H=C), 19.5 (CH_3). ^{19}F NMR (376 MHz, DMSO-d_6): -110.09 (m, C_6H_4-F).

2.5. General procedure for the synthesis of complexes 4-11

To a Schlenk tube containing a solution of the desired half-unit **1**, **2** or **3** in 10 mL of ethanol, was added under stirring, a solution of the substituted salicylaldehyde dissolved in 5 mL of ethanol. The resulting solution was refluxed for 1 h, and at room temperature a solution of the hydrated metal(II) acetate dissolved in 5 mL of ethanol was added. The resulting mixture was refluxed for 4 h. The dark suspension was subsequently cooled at -30 °C for 4 h. The dark solid material was filtered off, washed with three 4 mL portion of cold ethanol and three 4 mL portion of diethyl ether. Finally, the solid was dried under vacuum for 2 h.

2.5.1. [Ni{(4-CH_3O-C_6H_4)C(=O)CH=C(CH_3)N-*o*-C_6H_4N=CH-(2-O,4-CH_3O-C_6H_3)}] (4)

Half-unit ligand **1**: 200 mg (0.708 mmol), 4-Methoxysalicylaldehyde: 108 mg (0.708 mmol) and nickel(II) acetate tetrahydrate: 264.3 mg (1.062 mmol); yield: 232 mg (69.2%).of a dark red powder. Recrystallization carried out in an open Erlenmeyer under a fume Hood by slow diffusion of pentane into a saturated dichloromethane solution of **4** deposited dark red single crystals suitable for X-ray structure determination. M.p. 227-229 °C. Anal. calcd for $C_{25}H_{22}N_2NiO_4 \cdot H_2O$ (491.19 g mol^{-1}): C, 61.13; H, 4.93; N, 5.70. Found: C, 60.80; H, 4.87; N, 5.49. FT-IR (KBr pellet, cm^{-1}): 3580(m), 3422(m), ν(O–H), 2956(w), 2932(w), 2836(w) ν(C–H),1608(vs),1546(vs), 1498(s) ν(C⋯O), ν(C⋯N) and/or ν(C⋯C),1250(s),1216(s) ν(C-O). ^{1}H NMR (400 MHz, DMSO-d_6): 8.54 (s, 1 H, N-CH), 7.93 (d, J = 7.9 Hz, 1 H, H3-sal), 7.83 (d, J = 8.0 Hz, 2 H, *4*-$C_6H_4OCH_3$), 7.46 (dd, J = 8.2 and 2.5 Hz, 2 H, *2*-C_6H_4), 7.09 (qd, J = 8.0 and 4.0 Hz, 2 H, *2*-C_6H_4), 6.97 (d, J = 8.0 Hz, 2 H, *4*-$C_6H_4OCH_3$), 6.33 (d, J = 8.7 Hz, 1 H, H6-sal), 6.31 (dd, J = 8.7 and 2.4 Hz, 1 H, H5-sal), 6.16 (s, 1 H, CH=C), 3.81 (s, 3 H, C_6H_3-OCH_3), 3.76 (s, 3 H, *4*-$C_6H_4OCH_3$), 2.50 (s, 3 H, CH_3). ^{13}C{^{1}H} NMR (101 MHz, DMSO-d_6): 172.4 (C=O), 166.7 (CH=*C*), 165.3(C_6-OCH_3) , 165.1 (C_6-OCH_3), 161.3 (C2-sal), 153.5 (N=CH), 143.7 (C-N, *2*-C_6H_4), 142.6 (C-N, *2*-C_6H_4), 135.0 (CH, *2*-C_6H_4), 128.7 (CH, *4*-$C_6H_4OCH_3$), 128.3 (C_{quat}, *4*-C_6H_4-CO), 125.3 (CH, *2*-C_6H_4), 123.4 (CH, *2*-C_6H_4), 121.7 (CH, *2*-C_6H_4), 115.2 (C_{quat}, CH_3O-C_6H_3-CH), 115.0 (CH, C_6H_3), 113.5 (CH, *4*-$C_6H_4OCH_3$), 107.0 (CH, C_6H_3), 101.3 (*C*H=C), 101.2 (CH, C_6H_3), 55.3 ($C_6H_3OCH_3$), 55.1 (*4*-$C_6H_4OCH_3$), 24.6 (CH_3).

2.5.2. [Cu{(4-CH_3O-C_6H_4)C(=O)CH=C(CH_3)N-o-C_6H_4N=CH-(2-O,4-CH_3O-C_6H_3)}] (5)

Half-unit ligand **1**: 200 mg (0.708 mmol), 4-Methoxysalicylaldehyde: 108 mg (0.708 mmol) and copper(II) acetate monohydrate: 212 mg (1.063 mmol); yield: 314 mg (93.1%) of Dark green powder. Recrystallization by slow diffusion of pentane into a saturated pyridine/dichloromethane (1:1) mixture of **5** deposited dark green single crystals suitable for X-ray structure determination. M.p. 181-183 °C. Anal. calcd for $C_{25}H_{22}CuN_2O_4$ (477.99 g mol^{-1}): C, 62.82; H, 4.64; N, 5.86. Found: C, 62.56; H, 4.77; N, 6.28. HRMS-ESI$^+$ (based on $C_{25}H_{22}N_2O_4Na^{63}Cu$ $[M^+Na]^+$) m/z calcd: 500.07678; found: 500.0771 (1 ppm). FT-IR (KBr pellet, cm^{-1}): 3061(w), 2998(w), 2957(w), 2929(w) ν(C–H), 1605(vs), 1554(w), 1499(s) ν(C⋯O), ν(C⋯N) and/or ν(C⋯C), 1244(s), 1209(s) ν(C-O).

2.5.3. [Ni{(η^5-C_5H_5)Fe(η^5-C_5H_4)-C(O)CH=C(CH_3)N-o-C_6H_4N=CH-(2-O,5-CH_3O-C_6H_3)}] (6)

Half-unit ligand **3**: 200 mg (0.555 mmol), 5-Methoxysalicylaldehyde: 69.3 µL (0.555 mmol) and nickel(II) acetate tetrahydrate: 207.2 mg (0.834 mmol); yield: 207 mg (67.7%) of a violet solid. M.p. 145-147 °C. Anal. Calcd for $C_{28}H_{24}N_2FeNiO_3 \cdot CH_3CH_2OH$ (596.10 g mol^{-1}): C, 60.34; H, 5.06; N, 4.69. Found: C, 60.60; H, 4.99; N, 4.66. FT-IR (KBr pellet, cm^{-1}): 3400(m), *v* (O-H); 3076(w), 3004(w), 2990(w) *v*(C-H aryl), 2970(m), 2892(m), 2838(m) *v*(C-H alkyl), 1600(s), 1516(vs), 1488(s) *v*(C⋯N), *v*(C⋯O) and/or *v*(C⋯C), 1288(s), 1266(s), 1254(s), 1216(s) *v*(C-O). ^{1}H NMR (400 MHz, $CDCl_3$): 8.12 (s, 1 H, N=CH), 7.61 (d, *J* = 8.1 Hz, 1 H, C_6H_3), 7.28 (d, *J* = 8.2 Hz, 1 H, *2*-C_6H_4), 7.10-6.92 (m, 4 H, *2*-C_6H_4 + C_6H_3), 6.70 (d, *J* = 2.8 Hz, 1 H, H6-sal), 5.64 (s, 1 H, CH=C), 4.76 (m, 2 H, C_5H_4), 4.35 (m, 2 H, C_5H_4), 4.20 (s, 5 H, C_5H_5), 3.77 (s, 3 H, OCH_3), 2.44 (s, 3 H, CH_3).^{13}C{^{1}H} NMR (101 MHz, $CDCl_3$): 180.3 (C=O), 162.3 (CH=*C*), 161.7 (N=CH), 152.0 (C2-sal), 149.7 (C5-sal), 145.3 (CN, *2*-C_6H_4), 142.7 (CN, *2*-C_6H_4), 126.1, 123.1, 122.9 (CH, *2*-C_6H_4 + C_6H_3), 121.8 (CH, *2*-C_6H_4), 118.8 (C1-sal), 114.4 (CH, C_6H_3), 111.3 (CH, C_6H_3), 102.9 (*C*H=C), 79.9 (C_{ipso}, C_5H_4), 70.7 (C_5H_4), 70.2 (C_5H_5), 68.8 (C_5H_4), 55.9 (OCH_3), 24.8 (CH_3).

2.5.4. [Cu{(η^5-C_5H_5)Fe(η^5-C_5H_4)-C(O)CH=C(CH_3)N-o-C_6H_4N=CH-(2-O,5-CH_3O-C_6H_3)}] (7)

Half-unit ligand **3**: 200 mg (0.555 mmol), 5-Methoxysalicylaldehyde: 69.3 µL (0.555 mmol) and copper(II) acetate monohydrate: 166.2 mg (0.834 mmol); yield: 234 mg (76.2%) of red wine powder. Recrystallization by slow diffusion of pentane into a saturated metanol/dichloromethane (1:1) mixture of **7** deposited a dark brown single crystals suitable for X-ray structure determination. M.p. 163-165 °C. Anal. Calcd for $C_{28}H_{24}CuFeN_2O_3 \cdot CH_3OH$ (587.93 g mol^{-1}): C, 59.24; H, 4.80; N, 4.76. Found: C, 59.33; H, 4.80; N, 4.81. HRMS-ESI$^+$ (based on $C_{28}H_{24}N_2O_3Na^{56}Fe^{63}Cu$ $[M^+Na]^+$) m/z calcd: 578.03245; found: 578.0327 (0 ppm). FT-IR (KBr pellet, cm^{-1}): 3078(w), 2996(w) ν(C-H aryl), 2968(w) 2926(m), 2898(w), 2834(w) ν(C-H alkyl), 1600(s), 1513(vs), 1474(s) ν(C$\cdots$N), ν(C$\cdots$O) and/or ν(C$\cdots$C), 1286(s), 1266(s), 1254(s), 1214(s) ν(C-O).

2.5.5. [Ni{(4-F-C_6H_4)C(O)CH=C(CH_3)N-o-C_6H_4N=CH-(2-O,3,5-F_2-C_6H_2)}] (8)

Half-unit ligand **2**: 200 mg (0.740 mmol), 3,5-difluorosalicylaldehyde: 117 mg (0.740 mmol) and nickel(II) acetate tetrahydrate: 276.2 mg (1.063 mmol); yield: 246 mg (71.2%). of a brown powder. M.p. 184-186 °C Anal. Calcd for $C_{23}H_{15}F_3N_2NiO_2$ (467.07 g mol^{-1}): C, 59.14; H, 3.24; N, 6.00. Found: C, 59.03; H, 3.34; N, 5.77. HRMS-ESI$^+$ (based on $C_{23}H_{15}N_2O_2F_3Na^{58}Ni$ $[M^+Na]^+$) m/z calcd: 489.03313; found: 489.0331 (0 ppm). FT-IR (KBr pellet, cm^{-1}): 3432(w), ν(O-H); 3076(vw), 3028(w), ν(C-H aryl), 2966(vw), 2924(vw) ν(C-H alkyl), 1602(s), 1546(s), 1482(vs) ν(C$\cdots$N), ν(C$\cdots$O) and/or ν(C$\cdots$C), 1378 (vs), 1326(vw), 1260(s) ν(C-F). ^{1}H NMR (400 MHz, DMSO-d_6): 9.73 (s, 1 H, N=CH), 7.98 (d, J = 8.0 Hz, 1 H, 2-C_6H_4), 7.89 (q, J=4.0 Hz, 2 H, C_6H_4-F), 7.52 (d, J = 8.0 Hz, 1 H, 2-C_6H_4), 7.35 (d, J = 8.0 Hz, 1 H, 2-C_6H_4), 7.30–7.16 (m, 4 H, C_6H_4F + $C_6H_2F_2$), 7.11 (d, J = 8.0 Hz, 1 H, 2-C_6H_4), 6.21 (s, 1 H, CH=C), 2.53 (s, 3 H, CH_3). ^{13}C{^{1}H} NMR (101 MHz, DMSO-d_6): 171.7 (C=O), 166.5 (CH=*C*), 166.3 (d, $^1J_{CF}$=249.0 Hz, C_6H_4F), 154.9 (C2-sal), 154.4 (d, $^1J_{CF}$ = 256.0 Hz, $C_6H_2F_2$), 150.9 (N=CH), 149.8 (d, $^1J_{CF}$ = 213.0 Hz, $C_6H_2F_2$), 143.3 (CN, 2-C_6H_4), 141.2 (CN, 2-C_6H_4), 134.1 (C_{quat}, C_6H_4F), 129.5 (d, $^3J_{CF}$ = 9.0 Hz, C_6H_4F), 127.3 , 124.2 , 122.8 (*CH*, 2-C_6H_4), 120.4 (C_{quat}, C1-sal), 116.3 (*CH*, 2-C_6H_4), 115.3 (d, $^2J_{CF}$ = 21.0 Hz, C_6H_4F), 111.5 (d, $^2J_{CF}$ = 24.0 Hz, $C_6H_2F_2$), 109.3 (dd, $^2J_{CF}$ = 24.0 Hz, $C_6H_2F_2$), 102.2 (*C*H=C), 26.6 (CH_3). ^{19}F (376 MHz, DMSO-d_6): -109.7 (q, J_{FH} = 7.5 Hz, C_6H_4-F), -128.1 (q, J_{FH} = 7.5 Hz, $C_6H_2F_2$), -129.7 (t, J_{FH} = 11.0 Hz, $C_6H_2F_2$).

2.5.6. [Cu{(4-F-C_6H_4)C(O)CH=C(CH_3)N-o-C_6H_4N=CH-(2-O,3,5-F_2-C_6H_2)}] (9)

Half-unit ligand **2**: 200 mg (0.740 mmol), 3,5-difluorosalicylaldehyde: 117 mg (0.740 mmol) and copper(II) acetate monohydrate: 221.6 mg (1.063 mmol); yield: 290 mg (81.5%) of a dark green powder. Recrystallization by slow diffusion of pentane into a saturated metanol/dichloromethane (1:1) mixture of **9** deposited a dark green single crystals suitable for X-ray structure determination. M.p. 191-193 °C Anal. Calcd for $C_{23}H_{15}CuFN_3O_2$ (480.93 g mol^{-1}): C, 57.44; H, 3.35; N, 8.74. Found: C, 57.51; H, 3.44; N, 8.40. FT-IR (KBr pellet, cm^{-1}): 3068(vw), 3012(w) ν(C-H aryl), 2974(vw), 2928(vw) ν(C-H alkyl), 1606(s), 1544(s), 1476(vs) ν(C=N), ν(C=O) and/or ν(C=C), 1456 (vs), 1368(vw), 1294(m) ν(C-F).

2.5.7. [Ni{(4-F-C_6H_4)C(O)CH=C(CH_3)N-o-C_6H_4N=CH-(2-O,5-NO_2-C_6H_3)}] (10)

Half-unit ligand **2**: 200 mg (0.740 mmol), 5-nitrosalicylaldehyde: 124 mg (0.740 mmol) and nickel(II) acetate tetrahydrate: 276.2 mg (1.063 mmol); yield: 227 mg (64.4%) of a dark orange powder. M.p. 201-203 °C (dec). Anal. Calcd for $C_{23}H_{16}FN_3NiO_4$ (476.08 g mol^{-1}): C, 58.02; H, 3.39; N, 8.83. Found: C, 56.87; H, 3.40; N, 8.34. HRMS-ESI$^+$ (based on $C_{23}H_{16}N_3O_4FNa^{58}Ni$ $[M^+Na]^+$) m/z calcd: 498.03705; found: 498.0369 (0 ppm). FT-IR (KBr pellet, cm^{-1}): 3432(w), ν(O-H), 3066(w) ν(C-H aryl), 2920(vw) ν(C-H alkyl), 1604(s), ν (C=N), ν(C=O) and/or ν(C=C), 1542(s) 1492(vs), 1410(S), 1378(s), 1318(s) ν_{asym} (NO_2), ν_{sym} (NO_2) and/or ν(C-F). Attempts to Recrystallize **10** by slow diffusion of dichloromethane into a saturated pyridine solution in air deposited a few yellow single crystals of [$NiCl_2(py)_4$] identified by X-ray structure determination.

2.5.8. [Cu{(4-F-C_6H_4)C(O)CH=C(CH_3)N-o-C_6H_4N=CH-(2-O,5-NO_2-C_6H_3)}] (11)

Half-unit ligand **2**: 200 mg (0.740 mmol), 5-nitrosalicylaldehyde: 124 mg (0.740 mmol) and copper(II) acetate monohydrate: 221.6 mg (1.063 mmol); yield: 290 mg (81.5%) of a brown powder. Recrystallization by slow diffusion of pentane into a saturated pyridine solution of **11** deposited brown single crystals suitable for X-ray structure determination. M.p. 205-207 °C (dec). Anal.Calcd for $C_{23}H_{16}CuFN_3O_4$ (480.94 g mol^{-1}): C, 57.44; H, 3.35; N, 8.74. Found: C, 58.32; H, 3.14; N, 8.87. HRMS-ESI$^+$ (based on $C_{23}H_{16}N_3O_4FNa^{63}Cu$ $[M^+Na]^+$) m/z calcd: 503.0313; found: 503.0312 (0 ppm). Ft-IR (KBr pellet, cm^{-1}): 3229(w) ν(O-H), 3061(vw) ν(C-H aryl), 2971 (w), 2920 (w) ν(C-H alkyl), 1599(w), 1546(s) ν(C=N), ν(C=O) and/or ν(C=C), 1494(s) 1492(vs), 1316(s) ν_{asym} (NO_2), ν_{sym}(NO_2) and/or ν(C-F).

2.6. X-ray Crystal Structure Determinations

Well-shaped single crystals of compounds **4**·H_2O, **5**·CH_2Cl_2, **7**·CH_3OH, **9**·$2CH_3OH$ and **11**, were mounted on top of glass fibers in a random orientation. Diffraction data were collected at 296(2) K on a Bruker D8 QUEST diffractometer equipped with a bidimensional CMOS Photon100 detector, using graphite monochromated Mo-Kα radiation (λ = 0.71073 Å). The diffraction frames were integrated using the APEX2 package [29], and were corrected for absorptions with SADABS. A yellow single crystal of $[NiCl_2(py)_4]\cdot 0.37H_2O$ was coated in Paratone-N oil, mounted on a Kaptan loop and transferred to the cold gas stream of the cooling device. Intensity data were collected at T = 150(2) K on a D8 VENTURE Bruker AXS diffractometer equipped with a multiplayers monochromated Mo-Kα radiation (λ = 0.71073 Å) and a CMOS Photon100 detector, and were corrected for absorption effects using multiscanned reflections. The structures of **4** and **7** were solved by direct methods using the OLEX 2 program [30], that of **5** was solved by Patterson methods [31], those of **9** and **11** were solved with OLEX2 structure solution program by charge flipping method [32], and that of $[NiCl_2(py)_4]\cdot 0.37H_2O$ was solved by direct methods using the *SIR97* program [33]. All the structures were then refined with full-matrix least-square methods based on F^2 (*SHELXL-97*) [31,34]. For the six compounds, non-hydrogen atoms were refined with anisotropic displacement parameters. All hydrogen atoms were included in their calculated positions, assigned fixed isotropic thermal parameters and constrained to ride on their parent atoms. A summary of the details about crystal data, collection parameters and refinement are documented in Table 1, and additional crystallographic details are in the CIF files. ORTEP views were drawn using OLEX2 software [30].

Table 1. Crystal data, details of data collection and structure refinement parameters for compounds **4**·OH_2, **5**·CH_2Cl_2, **7**·CH_3OH, **9**·$2CH_3OH$, **11** and $[NiCl_2(py)_4]\cdot 0.37H_2O$

	4·OH_2	**5**·CH_2Cl_2	**7**·CH_3OH	**9**·$2CH_3OH$	**11**	$NiCl_2(py)_4]\cdot 0.37H_2O$
Empirical Formula	$C_{25}H_{24}N_2NiO_5$	$C_{26}H_{24}Cl_2CuN_2O_4$	$C_{29}H_{28}CuFeN_2O_4$	$C_{25}H_{23}CuF_3N_2O_4$	$C_{23}H_{16}CuFN_3O_4$	$C_{20}H_{20.73}Cl_2N_4NiO_{0.37}$
Formula mass, g mol^{-1}	491.17	562.91	587.92	535.99	480.93	452.61
Collection T, K	296(2)	296(2)	296(2)	296(2)	296(2)	150(2)
crystal system	monoclinic	Triclinic	monoclinic	triclinic	Monoclinic	Tetragonal
space group	C2/c	P-1	$P2_1/c$	P-1	$P2_1/c$	$I4_1/a$
a (Å)	30.573(3)	7.3942(4)	13.329(3)	8.0752(3)	7.786(4)	15.8029(18)

b (Å)	7.2985(6)	12.9514(7)	24.948(5)	11.5973(4)	10.420(6)	15.8029
c (Å)	24.800(4)	13.1842(6)	7.4866(16)	12.5377(4)	25.034(13)	16.875(2)
α (°)	90	99.6020(10)	90	91.092(2)	90	90
β (°)	127.384(2)	97.8760(10)	97.244(7)	91.563(2)	95.86(2)	90
γ (°)	90	96.109(2)	90	98.749(2)	90	90
V (Å^3)	4397.0(8)	1222.31(11)	2469.7(9)	1159.75(7)	2020.5(18)	4214.3(11)
Z	8	2	4	2	4	8
D_{calcd} (g cm^{-3})	1.484	1.529	1.581	1.535	1.581	1.427
Crystal size (mm)	0.62 × 0.274 × 0.022	0.32 × 0.252 × 0.038	0.258 × 0.099 × 0.089	0.335 × 0.254 × 0.132	0.207 × 0.176 × 0.11	0.60 x 0.32 x 0.29
F(000)	2048.0	578.0	1212.0	550.0	980.0	1869
abs coeff (mm^{-1})	0.923	1.149	1.488	1.001	1.127	1.188
θ range (°)	5.34 to 49.88	4.918 to 52.81	4.48 to 52.84	4.76 to 52.88	4.238 to 52.754	3.025 to 27.460
range h,k,l	-36/36, -8/8, -29/29	-9/9, -16/16, -16/15	-16/16, -31/31, -9/9	-10/10, -14/14, -15/15	-9/9, -13/13, -31/30	-20/20, -20/20, -21/18
No. total refl.	19886	31380	98839	99600	20316	16008
No. unique refl.	3845	5009	3749	4766	4091	1212
R_{int}	0.0594	0.0690	0.0591	0.0295	0.1265	0.0291
Comp. θ_{max} (%)	99.7	99.4	99.7	99.7	97.7	99.9
Max/min transmission	0.742/1.000	0.661/0.745	0.758/0.927	0.869/1.000	0.839/1.000	0.709/0.494
Data/Restraints/Parameters	3845/0/304	5009/0/316	5066/0/338	4766/0/321	4091/0/290	1212 / 0 / 72
Final R						
[$I>2\sigma(I)$]	R_1 = 0.0605					
wR_2 = 0.1104	R_1 = 0.0505					
wR_2 = 0.1177	R_1 = 0.0258					
wR_2 = 0.0622	R_1 = 0.0261					
wR_2 = 0.0737	R_1 = 0.0486					
wR_2 = 0.0964	R_1 = 0.0256					
wR_2 = 0.0653						
R indices (all data)	R_1 = 0.0895					
wR_2 = 0.1226	R_1 = 0.0794					
wR_2 = 0.1369	R_1 = 0.0327					
wR_2 = 0.0656	R_1 = 0.0295					
wR_2 = 0.0769	R_1 = 0.0822					
wR_2 = 0.1070	R_1 = 0.0286					
wR_2 = 0.0686						
Goodness of fit / F^2	1.132	1.063	1.079	1.060	1.012	1.090
Largest diff. Peak/hole (eÅ^{-3})	0.65/-0.39	0.87/-0.69	0.30/-0.22	0.32/-0.22	0.32/-0.50	0.268/-0.421

2.7. Computational Details

DFT [35-38] calculations were carried out using the Amsterdam Density Functional (ADF 2012.01) program [39,40]. The Vosko-Wilk-Nusair parametrization [41] was used to treat electron correlation within the local density approximation, with gradient corrections added for exchange (Becke88) [42,43], and correlation (Perdew) [44,45], respectively (BP86 functional). The numerical integration procedure applied for the calculation was developed by Te Velde [37]. The standard ADF TZ2P basis set was used in all the calculations. The frozen core approximation was used at the following levels: Fe, 3p; Ni, 3p; Cu, 3p; C, 1s; N, 1s, O, 1s and F, 1s [37]. Spin-unrestricted calculations were carried out on the odd-electrons systems. Full geometry optimizations were carried out on each complex using the analytical gradient method implemented by Versluis and Ziegler [46], and its minimum energy was corroborated by inspecting their calculated vibrational spectra, finding no imaginary vibration frequencies. The UV-visible electronic absorption transitions were computed on the DFT-optimized geometries using the TD-DFT [47] method implemented within the ADF program, using the B3LYP functional [48,49].

3. Results and discussion

3.1. Syntheses

The anisyl- and 4-fluorophenyl-containing half-units **1** and **2** were synthesized, like their known ferrocenyl counterpart **3** [23], by monocondensation reaction of anisoylacetone and 4-fluorobenzoylacetone, respectively, with *o*-phenylene diamine in refluxing toluene for 6 h (Scheme 1). A Dean-Stark apparatus was used to remove the generated water and the progress of the reaction was monitored by TLC. High concentration of the reagents leads to the formation of benzodiazepines as side products [12c,50]. Compounds **1** and **2** were isolated as air and thermally stable yellow microcrystalline solids in reasonable yields of 64 and 57%, respectively. They are soluble in dichloromethane, diethyl ether and ethanol but are insoluble in hydrocarbon solvents.

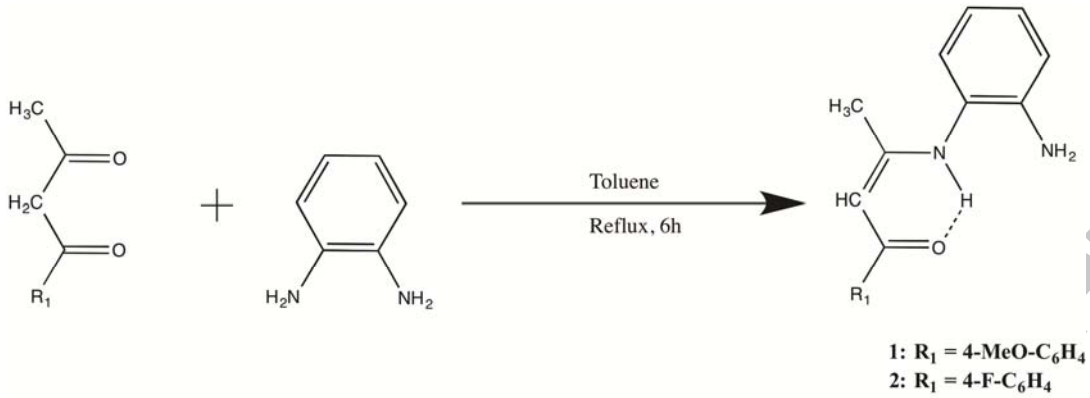

Scheme 1 Synthesis of the half-units **1** and **2**

The neutral unsymmetrically-substituted mono- and bimetallic Schiff base complexes **4-11** (Table 2) were prepared by reacting appropriate half-units **1-3**, an equimolar amounts of the desired substituted salicylaldehydes and either 1.5 equiv. of nickel(II) acetate tetrahydrate or copper(II) acetate monohydrate in refluxing ethanol for 4 h (Scheme 2). Complexes **4-11** were isolated as colored microcrystalline powders in yields ranging from 65 to 93% (see section 2.5 for details). They are air and thermally stable, moisture insensitive on storage under ordinary condition, and exhibit good solubility in common organic solvents except **10** and **11** that are poorly soluble but very soluble in pyridine. All compounds are not soluble in diethyl ether and hydrocarbon solvents.

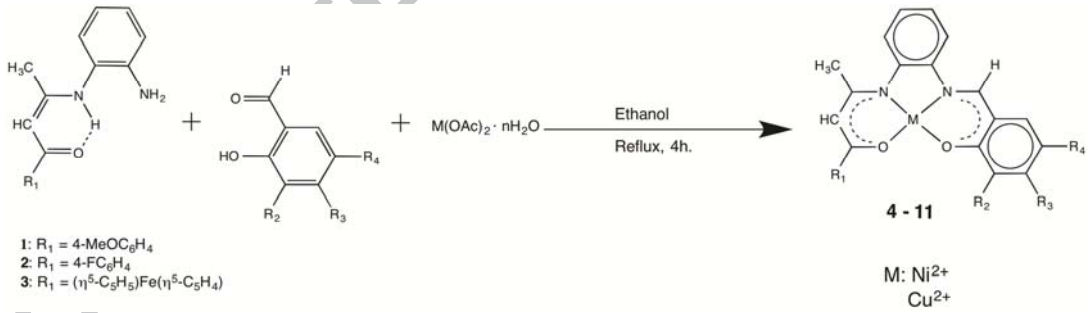

Scheme 2 Synthesis of complexes **4-11**

Table 2. Substitution pattern of the Schiff base complexes **4-11** prepared in this work

Compd.	M	R^1	R^2	R^3	R^4	Yield (%)
4	Ni	*4*-MeO-C_6H_4-	H	OMe	H	69
5	Cu	*4*-MeO-C_6H_4-	H	OMe	H	93
6	Ni	(η^5-C_5H_5)Fe(η^5-C_5H_4)	H	H	OMe	68
7	Cu	(η^5-C_5H_5)Fe(η^5-C_5H_4)	H	H	OMe	76
8	Ni	*4*-F-C_6H_4-	F	H	F	71
9	Cu	*4*-F-C_6H_4-	F	H	F	81
10	Ni	*4*-F-C_6H_4-	H	H	NO_2	64
11	Cu	*4*-F-C_6H_4-	H	H	NO_2	81

The composition and structures of the half-unis **1** and **2**, and of complexes **4**-**11** were established by satisfactory elemental analyses, FT-IR and NMR spectroscopy, and mass spectrometry (see experimental section for details). In addition, the crystal structures of **4**, **5**, **7**, **9** and **11** were determined by single crystal X-ray diffraction (see below). ESI^+ mass spectra of the half-units **1** and **2**, and of complexes **5**, **7**, **8**, **10** and **11** showed the presence of the molecular ion peaks with 100% intensity, and with the envelope of the isotopic pattern in good agreement with the simulated ones.

3.2. Infrared spectra

Solid-state FT-IR spectra of **1** and **2** exhibit similar pattern suggesting that both compounds have the same atom connectivity. For example, the two absorption bands observed between 3450 and 3370 cm^{-1} are due to the asymmetrical and symmetrical stretching modes of the terminal NH_2 group [51a]. A medium intensity band attributable to the *ν*(N–H) vibration is also seen at 3356 and 3348 cm^{-1}, respectively, suggesting that the enamine tautomer is the predominant form in the solid state [22,23,52]. The characteristic strong *ν*(C⋯O), *ν*(C⋯N) and/or *ν*(C⋯C), stretching vibrations of the enaminone core appear about 1600 cm^{-1}. Moreover, strong *ν*(C-O) and *ν*(C–F) vibrations are also observed at 1256 and 1310 cm^{-1} for **1** and **2** [51b], respectively, along with C-H bending mode vibrations around 750 cm^{-1}, typical of 1,2- and 1,4- disubstituted aromatic rings [51c].

On the other hand, the solid-state FT-IR spectra of complexes **4**-**11** are similar to those we have previously described for unsymmetrically-substituted tetradentate N_2O_2 species [13,20,24,25], exhibiting the characteristic ν(C⋯O), ν(C⋯N) and ν(C⋯C) stretching pattern about 1600 cm^{-1} of the organic Schiff base skeleton (see section 2.5 for details). Compounds **4**-**7** show an absorption band around 1260 cm^{-1} assigned to the C-O vibration of the methoxy

substituent of anisyl and salicylidene rings. In the spectra of complexes **8** and **9**, strong bands due to C-F vibrations are seen near 1300 cm^{-1}. Those bands also present in the spectra of **10** and **11** are partially masked by the strong intensity band between 1490-1300 cm^{-1} due to the asymmetrical and symmetrical vibration mode of the nitro group bore by these two latter complexes [51d].

3.3. NMR spectroscopy

The ^{1}H NMR spectra of the Half- unit **1** and **2**, and of the diamagnetic derived tetradentate Ni(II) complexes **4**, **6** and **8** were acquired at 298 K and exhibited the expected resonance patterns consistent with the proposed structures (see section 2.5 for complete assignments). Owing to its lack of solubility in all common deuterated solvents, no NMR spectra of **10** could be obtained. Attempts to record a ^{1}H NMR spectrum in pyridine-d_5 was also unsuccessful. The spectrum showed unassignable broad and shifted signals due to *in situ* generated paramagnetic five- or more probably six-coordinated Ni(II) species. $[NiCl_2(py)_4]$ was isolated upon recrystallization of **10** from a pyridine dichloromethane mixture (see sections 2.5.7 and 3.4).

The ^{1}H NMR spectra of **1** and **2** recorded in deuterated DMSO showed unshielded amino proton signals at 12.40 and 12.43 ppm, respectively, due to intramolecular hydrogen bonding between the secondary amine N-H and the oxygen atom of the carbonyl unit, thus closing a *pseudo* six-membered heterocycle [53,54a,b]. These downfield positions clearly indicate that both compounds exist as their enaminone tautomeric forms in solution. This is confirmed by the resonances of the methine proton at 6.01 and 6.05 ppm, respectively, and contrasts with the 60/40 keto-enamine/keto-imine tautomeric mixture found for the ferrocene-containing half-unit **3** in acetone-d_6 [23]. This different behavior could arise from the nature of the solvents used that is known to influence the position of the tautomeric equilibrium [54]. Spectra of **1** and **2** exhibit also a pair of singlets at 4.98/1.95 and 5.02/1.97 ppm (integral ratio 2:3) assigned to the NH_2 and methyl protons. In addition, the methoxy protons of the anisyl entity show up at 3.82 ppm in the ^{1}H NMR spectrum of **1**, whereas the 4-fluorophenyl group is identified by a multiplet centered at -110.09 ppm in the ^{19}F NMR spectrum of **2**.

The ^{1}H NMR spectra of the three diamagnetic Ni(II) complexes **4**, **6** and **8** show the presence of the N=CH azomethine proton resonating as 8.54, 8.12 and 9.73 ppm, respectively, bearing testimony of the assembly of the tetradentate Schiff base ligands [13,22, 24,25]. This is confirmed by the characteristic multiplicity patterns observed in the aromatic region of the 3-, 4- and 5-substituted salicylidene rings, and by the fact that the peculiar resonances of the

respective starting half-units are also reproduced in the spectra of the three complexes (see Section 2.5). For instance: (i) for **4**, the two methoxy substituents of the salicylidene and anisyl rings are seen at 3.81 and 3.76 ppm, respectively; (ii) for **6**, four sharp singlets appear at 2.47, 3.77, 4.20 and 5.64 ppm (integral ratio 3:3:5:1) due to the methyl, methoxy, free cyclopentadienyl ring and methine protons, respectively, and (iii) in the ^{19}F NMR spectrum of **8**, the three magnetically non equivalent fluorine nuclei of the 4-fluorophenyl and 3,5-difluorosalicylidene rings resonate at -109.7, -128.1 (5-F) and -129.7 (3-F) ppm [25b], respectively. Lastly, one can also note that the unsymmetrical nature of complexes **4**, **6** and **8**, as well as that of half-units **1** and **2**, is illustrated by the four differents resonances of various multiplicity observed for the four magnetically non-equivalent protons of the *o*-phenylene bridge in the range 6.5 to 7.8 ppm (see Section 2.5).

This unsymmetrical nature of the five compounds is confirmed by their proton decoupled ^{13}C NMR spectra, showing that each type of carbon gives rise to a separate resonance (see Section 2.5 for complete assignments). Specifically, in **2** and **8** the carbons bearing a fluorine substituent appear as doublets with $^{1}J_{CF}$ coupling constants ranging from 213 to 256 Hz. In **8**, the carbons located in 1,2 position of the C-F units give also rise to doublets with $^{2}J_{CF}$ of 24 Hz. A doublet is also observed for the *meta* carbon of the 4-fluorophenyl ring with a $^{3}J_{CF}$ of 9 Hz. Moreover, the spectra of **1** and **2** clearly support the existence of their keto–enamine tautomeric form with the methine carbon resonating at 92.5 and 92.7 ppm, respectively. Those chemical shifts are similar to that measured for their ferrocene-containing counterpart **3** (94.5 ppm) [23]. In complexes **4**, **6** and **8**, both the methine and carbonyl carbons experienced an upfield shift of 9 and 14 ppm, respectively, upon coordination of the half-units to the Ni(II) center and formation of the tetradentate complexes. The central enamine carbon is not affected by the complexation, showing only a very slight downfield shift of 1-4 ppm.

3.4. Crystal structures

Diffraction-quality single crystals for X-ray structure investigation were obtained for compounds **4**, **5**, **7**, **9** and **11**, by diffusion of pentane into, or slow evaporation of a saturated solution of the compound (see Section 2.5 for solvents used). The molecular structures are displayed in Figs. 1-4, crystal data are summarized in Table 1, selected bond lengths and angles of the [$M(N_2O_2)$] coordination core are given in Table 3 whereas other selected bond distances and angles are provided in Tables S1-S3 (Supplementary material). Complex **4** crystallizes as the hydrated compound **4**·H_2O, while complexes **5**, **7** and **9** crystallize as solvated dichloromethane or methanol compounds **5**·CH_2Cl_2, **7**·CH_3OH and **9**·$2CH_3OH$, respectively, with one molecular entity *per* asymmetric unit. All the complexes consist of a M(II)-centered unsymmetrically-substituted macroacyclic Schiff base core (M = Ni: **4**, Cu: **5**, **7**, **9** and **11**) substituted either by a pair of electron releasing (**4**, **5** and **7**) or electron withdrawing groups (**9** and **11**).

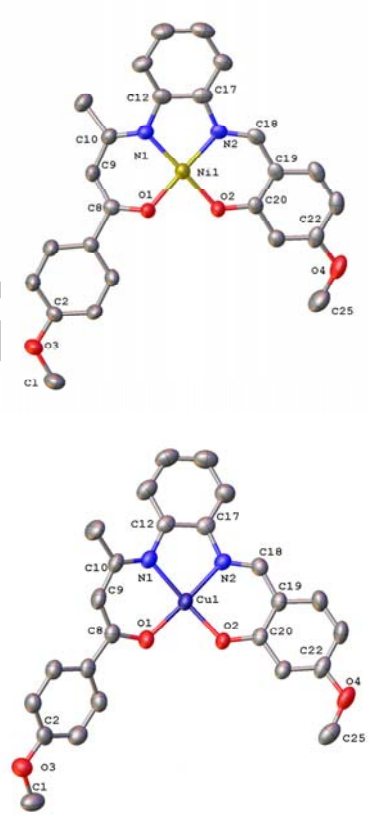

Fig. 1 Molecular structures of compounds **4**·H_2O (top) and **5**·CH_2Cl_2 (bottom) with partial atom labeling schemes. Hydrogens atoms and crystallization solvent molecules have been omitted for clarity. Thermal ellipsoids are drawn at 50% probability.

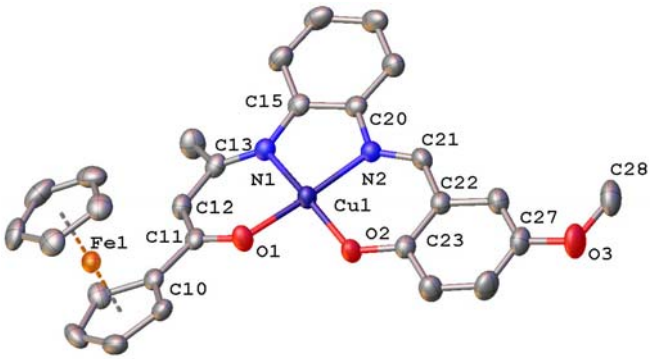

Fig. 2 Molecular structure of compound **7**·CH_3OH with partial atom labeling scheme. Hydrogen atoms and crystallization solvent molecule have been omitted for clarity. Thermal ellipsoids are drawn at 50% probability.

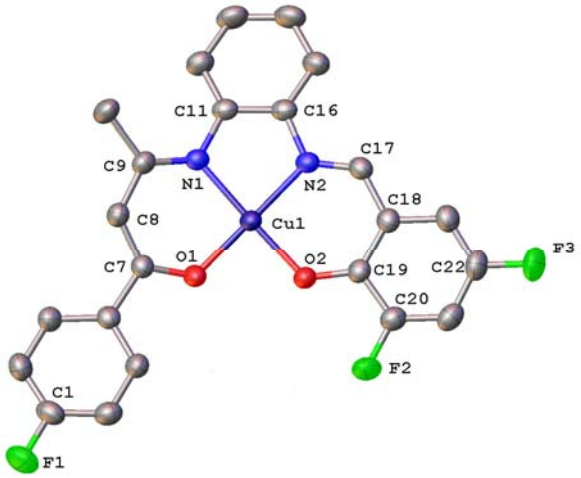

Fig. 3 Molecular structure of compound **9**·$2CH_3OH$ with partial atom labeling scheme. Hydrogen atoms and crystallization solvent molecules have been omitted for clarity. Thermal ellipsoids are drawn at 50% probability.

Compound **11** packs as centrosymmetric dimers resulting from apical short contact interaction of the Cu(II) metal ion of one molecule with a phenoxido oxygen atom of another N_2O_2-tetradentate ligand that is basal to the copper(II) center of the second complex (Figs. 4 and S1 in the Supplementary Material). The two halves of the dimeric entity are related by an inversion center located in the middle of the four membered Cu_2O_2 core. The axial and equatorial Cu(II)-O bond lengths in this asymmetric [Cu_2O_2] rhombic unit are of 2.63 and

1.935(2) Å, respectively, with a non-bonding Cu···Cu distance of 3.27Å. The Cu-O-Cu and O-Cu-O angles are of 89.92 and 90.08°, respectively, whereas the bridging [Cu_2O_2] plane makes a dihedral angle of 94.5° with the mean basal plane. This structural feature placing the Cu(II) metal ion in a square pyramidal environment was recently reported by us for four-coordinated [Cu(ONO +N)] Schiff base complexes [4c,55].

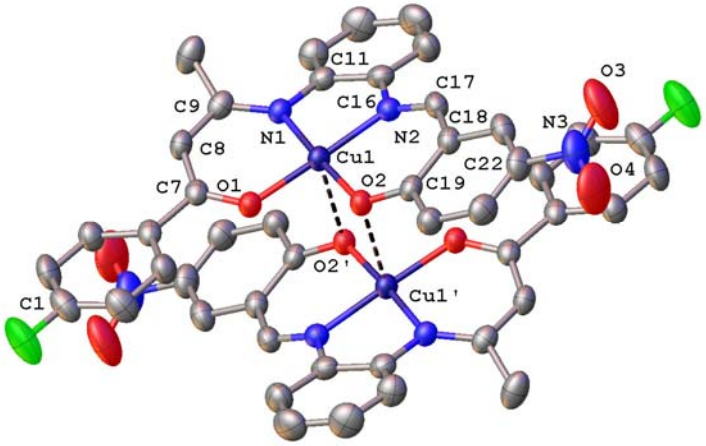

Fig. 4 Molecular structure of complex **11** showing partial atom numbering scheme and apical short contact Cu-O interactions in dashed-line. Hydrogen atoms are omitted for clarity. Thermal ellipsoids are drawn at 50% probability.

In each compound, the metal(II) ion is tetracoordinated with the coordination sphere formed by the amide and imine nitrogen atoms and the carbonyl and phenoxide oxygen atoms of the dianionic chelating tetradentate Schiff base ligand with respective cis-configuration (Figs. 1-4). Both the Ni(II)- and the Cu(II)-centered metal ions adopt a slightly distorted square planar geometry as reflected by the weak deviations (< 9°) from linearity of the two diagonal O-M-N angles (Table 3). The deviations of the Ni(II) metal center in **4**, and of Cu(II) metal ion in **5**, **7**, **9** and **11**, from the least-square N_2O_2 mean planes were found to be **0.021(2), 0.023(14), 0.041(8), 0.021(6) and 0.021(10) Å, respectively.** The metal-donor atom bond lengths range from 1.834(3) and 1.865(3) Å in **4** and from 1.8950(11) and 1.9608(19) Å in the Cu(II) derivatives **5**, **7**, **9** and **11** (Table 3). They are unexceptional and are in accordance with those reported in the literature for [Ni/Cu(N_2O_2)]-containing Schiff base compounds [2b,f,4c,6,13,22,24,25,53,55].

Table 3. Selected bond distances (Å) and angles (°)of the [M(N_2O_2)] coordination core for compounds **4**·OH_2, **5**·CH_2Cl_2, **7**·CH_3OH, **9**·2CH_3OH and **11** with their theoretically computed values into brackets

	4·H_2O	**5**·CH_2Cl_2	**7**·CH_3OH	**9**·2CH_3OH	**11**
Bond distances					
M(1)-O(1)	1.834(3) [1.876]	1.909(2) [1.955]	1.8997(15) [1.901]	1.8950(11) [1.952]	1.904(2) [1.950]
M(1)-O(2)	1.839(3) [1.881]	1.910(2) [1.959]	1.9142(15) [1.916]	1.9134(11) [1.957]	1.935(2) [1.964]
M(1)-N(1)	1.865(3) [1.899]	1.960(2) [1.996]	1.9604(17) [1.958]	1.9452(13) [1.991]	1.956(2) [1.991]
M(1)-N(2)	1.849(4) [1.870]	1.922(3) [1.996]	1.9246(17) [1.938]	1.9350(12) [1.972]	1.951(3) [1.974]
Angles					
O(1)-M(1)-N(2)	176.47(15) [178]	173.52(12) [176]	175.68(7) [178]	178.58(5) [175]	178.05(9) [176]
O(2)-M(1)-N(1)	173.98(17) [177]	171.15(12) [175]	170.79(7) [174]	178.11(5) [174]	177.21(9) [175]
O(1)-M(1)-O(2)	83.02(13) [83]	88.68(9) [89]	86.91(6) [87]	86.75(5) [89]	87.55(8) [89]
O(1)-M(1)-N(1)	95.54(15) [96]	93.86(10) [94]	94.79(7) [95]	94.76(5) [94]	95.18(9) [94]
O(2)-M(1)-N(2)	95.64(15) [95]	94.37(10) [94]	94.09(7) [94]	93.68(5) [94]	92.63(9) [93]
N(1)-M(1)-N(2)	86.12(16) [86]	83.98(11) [84]	84.89(7) [84]	84.78(5) [84]	84.62(10) [84]

M = Ni for **4**, Cu for **5**, **7**, **9** and **11**.

Complexation of the divalent nickel and copper ions by the dianionic tetradentate $[N_2O_2]^{2-}$ ligand generates three coplanar fused six-, five- and six-membered heterometallacycles (Figs 1-4). The six-membered heterometallacycles are held together by the five-membered diazametallacycle in which the N-C-C-N torsion angles are negligible (-3.8, 1.3, -0.8, 4.8 and -2.4 °, respectively). A peculiar feature of such unsymmetrically-substituted Schiff base derivatives having the *o*-phenylene spacer [20,24a,c,25b] is that the Werner-type coordination [M(N_2O_2)] core is also part of a bowed chelate Schiff base scaffold with angles formed by the two central carbons of the 6-membered chelate rings and the metal center of 168.0, 163.6, 170.6, 165.9 and 162.3°, respectively. Nevertheless, the metrical parameters measured in the three fused heterometallacycles are indicative of a π delocalization over the entire system (Tables S1-S3 in Supplementary material).

In **4** and **5**, the O=C-C=C-N keto-enamino plane makes dihedral angles of 19.9 and 13.8°, respectively, with the anisyl ring. Similar dihedral angles involving the 4-fluorophenyl substituent of 20.9 and 16.7° are found in compounds **9** and **11**, respectively. By contrast, in **7** the keto-enamino and the substituted cyclopentadienyl rings are almost coplanar (dihedral

angle = 6.2°), a feature we previously encountered for similar unsymmetrically-substituted tetradentate bimetallic Fe-Ni and Fe-Cu Schiff base complexes [13,20,24,25]. Moreover, in this latter complex the ferrocenyl unit adopts the classical linear η^5-Fe(II)-η^5 sandwich structure with parallel and staggered (15.4°) cyclopentadienyl rings. The ring centroid-iron-ring centroid angle is of 178.9°, and the ring centroid-iron distances are of 1.647 and 1.644 Å for the ring with and without the side chain, respectively.

On the other hand, the water, dichloromethane and methanol crystallization molecules found in the asymmetric units of **4**·H_2O, **5**·CH_2Cl_2, **7**·CH_3OH and **9**·$2CH_3OH$, respectively, interact in each case, through an intermolecular hydrogen bond with the O(2) phenolato oxygen atoms of the Schiff base pocket (Table S4 in the Supplementary Material). Such a hydrogen bonding with the phenolato oxygen atom seems to be a general trend in [M(N_2O_2)]-containing Schiff base complexes [20,24b,c,25a,56], as it is more basic than the carbonyl oxygen atom. In **4**·H_2O, the water molecule bridges two Ni(II) complexes through a second weaker hydrogen bond (Table S4) with the anisyl methoxy oxygen atom of the neighboring molecule (Fig. S2 in the Supplementary Material). A similar situation is observed in **5**·CH_2Cl_2 albeit the separations between the donor and acceptor atoms are rather large (3.289(5) and 3.401(6) Å). In addition to the intermolecular hydrogen bond noted above (Fig. S3 in the Supplementary Material), in **7**·CH_3OH one can note a apical interaction between Cu(1) and O(3) of the 4-methoxo substituent of the neighboring molecule (Fig. S4 in the Supplementary Material). This apical interaction of same nature to that we and others encountered previously [4c,6a], is weak (d_{Cu-O} = 3.29 Å) presumably due to the steric demand of the ferrocenyl fragment. Interestingly, in **9**·$2CH_3OH$ the second hydrogen bond (O(4)-H(4A)···O(3)) takes place between the two methanol crystallization solvents (Table S4 and Fig. S5 in the Supplementary Material).

On the other hand, recrystallization of a sample of **10** from a pyridine dichloromethane mixture deposited a few yellow crystals, of which a well shaped one was subjected to X-ray crystallographic analysis (see Section 2.6). In fact, it turned out to be the *trans*-tetrakis(pyridine) dichloronickel(II) hydrate derivative whose molecular structure is depicted in Fig. 5 with selected bond distances and angles given in the caption. Crystal data are summarized in Table 1. It crystallizes as the partially hydrated [$NiCl_2(py)_4$]·$0.37H_2O$ compound. The structure of [$NiCl_2(py)_4$]·$0.37H_2O$ is isostructural with the previously reported anhydrous [57] and $0.76H_2O$-hydrated [58] forms. In [$NiCl_2(py)_4$]·$0.37H_2O$, the

Ni(II) metal ion that lies on a rotoinversion 4-fold axis, adopts an elongated octahedral coordination geometry having two chlorine atoms in axial positions and four pyridine nitrogen atoms in equatorial positions, with Ni-Cl and Ni-N bond lengths of 2.4336(5) and 2.1195(12) Å. The N(1)-Ni(1)-N(1) angle is almost linear (179.03(6)°),while the Cl(1)-Ni(1)-Cl(1) angle is flat, being exactly 180.0°. The average N-Ni-Cl angle is 90.0 (3)º. The dihedral angle between the plane of the coordinated nitrogen atoms and the pyridine ring is 49.93º, each pyridine ring being rotated in the same (clockwise) direction. As expected, all those metrical parameters are in full accordance with those reported earlier for the anhydrous and hydrated $[NiCl_2(py)_4]$ species [57,58].

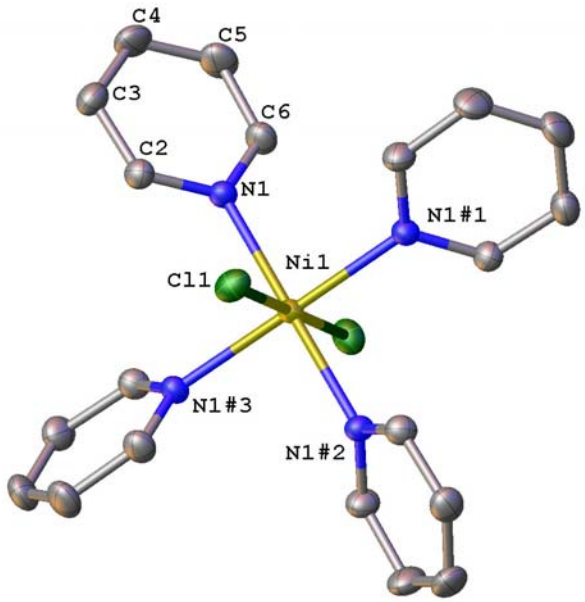

Fig. 5 Molecular structure of $[NiCl_2(py)_4]\cdot 0.37H_2O$ with atom labeling scheme. Hydrogens atoms and crystallization solvent molecule have been omitted for clarity. Thermal ellipsoids are drawn at 50% probability. Selected bond lengths (Å) and angles (°): Ni(1)-N(1) 2.1195(12), Ni(1)-Cl(1) 2.4336(5), N(1)-C(2) 1.3442(17), N(1)-C(6) 1.3377(18), C(2)-C(3) 1.380(2), C(3)-C(4) 1.381(2), C(4)-C(5) 1.378(2), C(5)-C(6) 1.388(2); N(1)-Ni(1)-Cl(1) 89.51(3), $N(1)^{\#1}$-Ni(1)-Cl(1) 90.49(3), N(1)-Ni(1)-$N(1)^{\#1}$ 89.94(6), N(1)-Ni(1)-$N(1)^{\#2}$ 179.03(6), N(1)-Ni(1)-$N(1)^{\#3}$ 90.07(6), Ni(1)-N(1)-C(2) 120.90(9), Ni(1)-N(1)-C(6) 121.68(10), C(2)-N(1)-C(6) 117.41(12). Symmetry transformations used to generate equivalent atoms: #1 -y+1/4, -x+1/4, -z+1/4; #2 y+3/4, x+5/4, -z+5/4; #3 -x+1, -y+1/2, z+1.

3.5. Electronic absorption spectroscopy

The electronic absorption spectra in the UV-visible region of the Schiff base complexes **4-11** were measured in two solvents of different dielectric constants (ε_r), CH_2Cl_2 (ε_r = 8.90) and in DMSO (ε_r = 47.6) (Fig. S9 in the Supplementary Material), and the experimental spectral data are collected in Table 4. In the 350-430 nm region, the spectra exhibit a strong broad absorption band for all the compounds, while a set of three absorption bands are observed in the 450-650 nm range. On passing from the less to the more polar solvent, those low-energy absorption bands are mainly blue shifted (Table 4), indicating a decrease of the dipole moment between the excited and the ground states. Based on computational TDDFT-assisted assignments (see section 3.7, Table 7), the high-energy band is attributed to intraligand charge transfer transitions (ILCT $\pi \rightarrow \pi^*$, and Fc$\rightarrow \pi^*$, transition in the case of bimetallic complexes **6** and **7).** The low-energy bands are assumed to originate from ligand-to-metal charge transfer (LMCT $\pi \rightarrow$M) and metal-to-ligand (MLCT M$\rightarrow \pi^*$) transitions. It is likely that square-planar Ni(II) and Cu(II)-complexes give rise to d-d transitions involved in the composition of the lowest energy band observed in the range 540-650 nm, as supported by TDDFT calculations in the case of **11** (Table 7).

Table 4 Experimental UV-vis absorption data for compounds **4-11**

Compd	λ/nm (log ε) CH_2Cl_2	λ/nm (log ε) DMSO	Solv. shift (cm^{-1})
4	376 (4.77)	374 (4.91)	-142
	444 (4.54)	440 (4.73)	-205
	541 (3.63)	554 (3.75)	+434
5	383 (4.42)	386 (4.35)	+203
	402 (4.46)	425 (4.18)	+1436
	601 (3.23)	595(3.30)	-287
6	384 (4.57)	384 (4.60)	0
	445 (3.94)	445 (4.19)	0
	495 (4.21)	495 (4.12)	0
	587 (3.55)	547 (3.81)	-1246
7	393 (4.69)	394 (4.50)	+65
	459 (4.47)	458 (4.33)	-48
	638 (3.28)	617 (3.18)	-533

8	374 (4.63)	372 (4.73)	-144
	452 (4.15)	456 (4.23)	+194
	492 (3.86)	457 (3.94)	-1557
	577 (3.51)	582 (3.59)	+149
9	384 (4.56)	390 (4.63)	+401
	405 (4.60)	438 (4.31)	+1860
	630 (3.24)	641 (2.80)	+272
10	369 (4.32)	362 (4.28)	-524
	402 (4.00)	380 (4.37)	-1440
	427 (4.23)	436 (4.34)	+483
	576 (3.31)	538 (3.56)	-1226
11	378 (4.62)	376 (4.69)	-141
	425 (4.12)	415 (4.52)	-567
	650 (3.03)	592 (2.82)	-1507

3.6. Electrochemical studies

The electrochemical behavior of the Schiff base complexes **4**-**11** has been investigated using cyclic voltammetry (CV) in CH_2Cl_2 solutions, at room temperature in a potential range of +0.65 to -2.20 V. The potentials are quoted against Ag/Ag^+ reference electrode. Interestingly, the CVs of the four Ni(II) complexes **4**, **6**, **8** and **10**, show an irreversible reduction wave (Fig. S15 in the Supplementary Material) while those of the four Cu(II) counterparts **5**, **7**, **9** and **11**, exhibit a reversible or quasi-reversible redox process (Fig. S16 in the Supplementary Material), attributed to the one-electron reduction of Ni(II) to Ni(I) [53,55,59] and to the Cu(II)/Cu(I) couple [18,53,55,60], respectively. The redox potentials are in accordance with the electron releasing and withdrawing ability of the substituents bore by the complexes (Table 5). As expected, in both Ni and Cu series complexes **4**-**7** bearing donor substituents are more difficult to reduce than **8**-**11** substituted with electron accepting groups (see Table 2 for substitution pattern). For instance, compare to **4** (MeO/MeO), **10** (F/NO_2) is much easier to reduce by 0.51 V; the same trend, albeit less pronounced (0.19 V), being observed between **5** and **11** (Table 5). Moreover, compound **10** is easier to reduce than **8** as it is the case for **11** compared to **9** indicating that the 5-nitro group exerts a more electron withdrawing effect than the 3,5-difluoro substituents, a feature we previously observed for

N_2O_2-tetradentate Ni(II) and Cu(II) Schiff base complexes [25b]. On the other hand, the CVs of the heterobimetallic complexes **6** and **7** present also reversible waves at amost similar potentials of 0.289 and 0.298 V, respectively (Fig. 6) due to the monoelectronic oxidation of the ferrocenyl fragment [61]. Those redox events are anodically shifted by ~90 mV with respect to free ferrocene. The increased difficulty to oxidize the Fe(II) center suggests that the substituted neutral side chain Schiff base complex acts as an electron withdrawing unit [13]. The anodic to cathodic peak-to-peak separations ($80 < \Delta E_p < 220$ mV) as well as the cathodic to anodic current ratios ($0.85 < i_{pc}/i_{pa} < 1.12$) remain close to the respective value measured for the internal ferrocene standard under the same electrochemical conditions (Table 5). The ΔE_p values are, however, significantly greater than the ideal value of 60 mV for a fully reversible one-electron process [62]. This may result from a combination of low solubility of some compounds, uncompensated solution resistance and presumably slow electron-transfer kinetics [62].

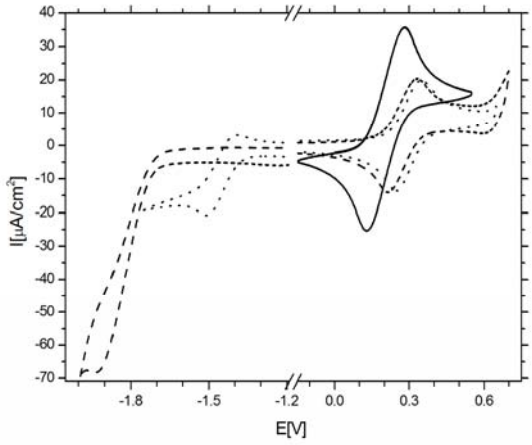

Fig. 6 Cyclic voltammograms of complexes **6** (dashed line) and **7** (dotted line), recorded in CH_2Cl_2 containing 0.1 M *n*-$Bu_4N^+PF_6^-$ at a vitreous carbon working electrode at 293 K, v = 100 mVs^{-1}, reference electrode Ag/Ag^+, internal reference $Cp_2Fe^{0/+}$ (solid line).

Table 5. Electrochemical data for the Schiff base complexes **4**-**11**[a]

Compd.	E_{pc} (V)	$E_{1/2}$/V (ΔE_p (mV))	i_{pc}/i_{pa}
4	-2.00	-	-
5	-	-1.43 (220)	0.85

6	-1.90	0.289 (113)	1.04
7	-	0.298 (93) -1.49 (110)	1.03 0.98
8	-1.71	-	-
9	-	-1.30 (130)	1.12
10	-1.49	-	-
11	-	-1.24 (80)	1.02
Cp_2Fe	-	0.203 (139)	0.9

[a] recorded in CH_2Cl_2 containing 0.1 M *n*-$Bu_4N^+PF_6^-$ as supporting electrolyte, at a vitreous carbon working electrode at 293 K with scan rate of 100 mV s^{-1}, reference electrode Ag/Ag^+.

3.7. Theoretical Investigations

A Density Functional Theory (DFT) investigation has been performed on compounds **4**-**11** in order to obtain a better understanding of their structure and electronic properties (see Section 2.7 for computational details). Their fully optimized molecular structures are shown in Fig. 7. The calculated bond distances and angles of **4**, **5**, **7**, **9** and **11** for which the single-crystal X-ray structures have been determined, are given into square brackets in Table 3, along with the experimental values, highlighting an overall good agreement between the X-ray and optimized structures. The optimized geometries of the Ni(II) derivatives **6**, **8** and **10** (Fig. 7) were computed based on their structurally characterized Cu(II) counterparts **7**, **9** and **11**, respectively. Their calculated bond distances and angles are provided in Tables S5-S7 (Supplementary Material). Moreover, calculations nicely reproduce the slight distortion of the square planar environment of the central divalent metal ions as well as the eclipsed conformation of the two cyclopentadienyl rings of ferrocene in both **6** and **7**.

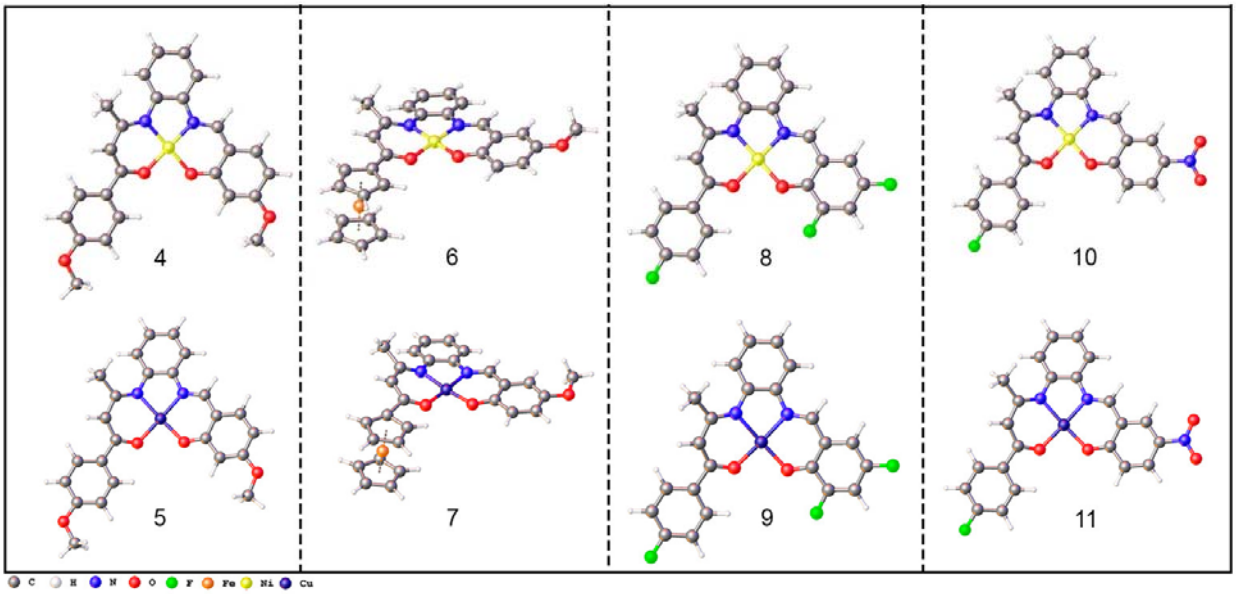

Fig. 7 Optimized geometries of the Schiff base complexes **4-11**

The molecular orbital diagrams of compounds **4, 6, 8, and 10** are displayed in Fig. 8 (see also Figs. S17-S24), with some pertinent computed data presented in Table 6. Analysis of the frontier molecular orbitals shows that the energy difference between HOMO and LUMO in Ni(II) complexes **4**, **8** and **10** have similar values, 1.50, 1.41 and 1.49 eV, respectively. This energy gap (1.38 eV) is somewhat lower in **6**, being mainly due to the contribution of the ferrocenyl fragment in the construction of the MO (HOMO 67%), thus reducing the HOMO-LUMO gap [13a,63]. Another important aspect is that these values are slightly greater than those computed for previously reported Schiff bases compounds with similar structure [13a,63]. A possible explanation could come from the nature of complexes **4-11** bearing either a pair of donor or acceptor substituents forming D-π-D and A-π-A systems, respectively, compared to D-π-A systems having the same [$M(N_2O_2)$] coordination core [53].

Table 6. Relevant Computed Data for Compounds **4-11**

	4	**5**	**6**	**7**	**8**	**9**	**10**	**11**
ΔE HOMO-LUMO (eV)	1.50	-	1.38	-	1.41	-	1.49	-
				Mulliken charges				
M	0.438	0.600	0.435	0.594	0.447	0.604	0.448	0.604
Fe	-	-	-0.030	-0.030	-	-	-	-
L			-	-				
				% localization in HOMO/(SOMO)/LUMO				
M	55/36	(46)	13/32	(46)	49/30	(46)	51/27	(46)
Fe	-	-	58/1	-	-	-	-	-
L	36/47	(37)	12/44	(37)	42/58	(36)	39/57	(37)

M = Ni for **4**, **6**, **8** and **10**; Cu for **5**, **7**, **9** and **11**. L = ligand.

In the Ni(II) complexes **4**, **8** and **10**, the HOMO is mainly constituted by 3*d* block (55, 49 and 54%, respectively) mainly constituted by dπ orbital and π-type ligand orbitals mixed in an antibonding fashion. (Fig. 8). In the heterobimetallic complex **6**, the HOMO is primarily made of 3d orbitals of the iron atom (the highest component of the so-called "t_{2g}" set [63]), being constituted by 58% of "*d*" orbitals of the iron atom (Fig. 8). The nickel atom does also participate to the HOMO with a minor contribution of 13% of the d orbitals. Those results are in accordance with the cyclic voltammetry responses (see Section 3.6). Meanwhile, the LUMO for all compounds is mainly composed by the orbitals of the ligand (49, 44, 57 and 57%, respectively) of antibonding character, and by the $d_{x^2-y^2}$ orbital of the nickel atom (37, 32, 30 and 29%, respectively) (Fig. 8) (See Fig. S9-S16 for more details).

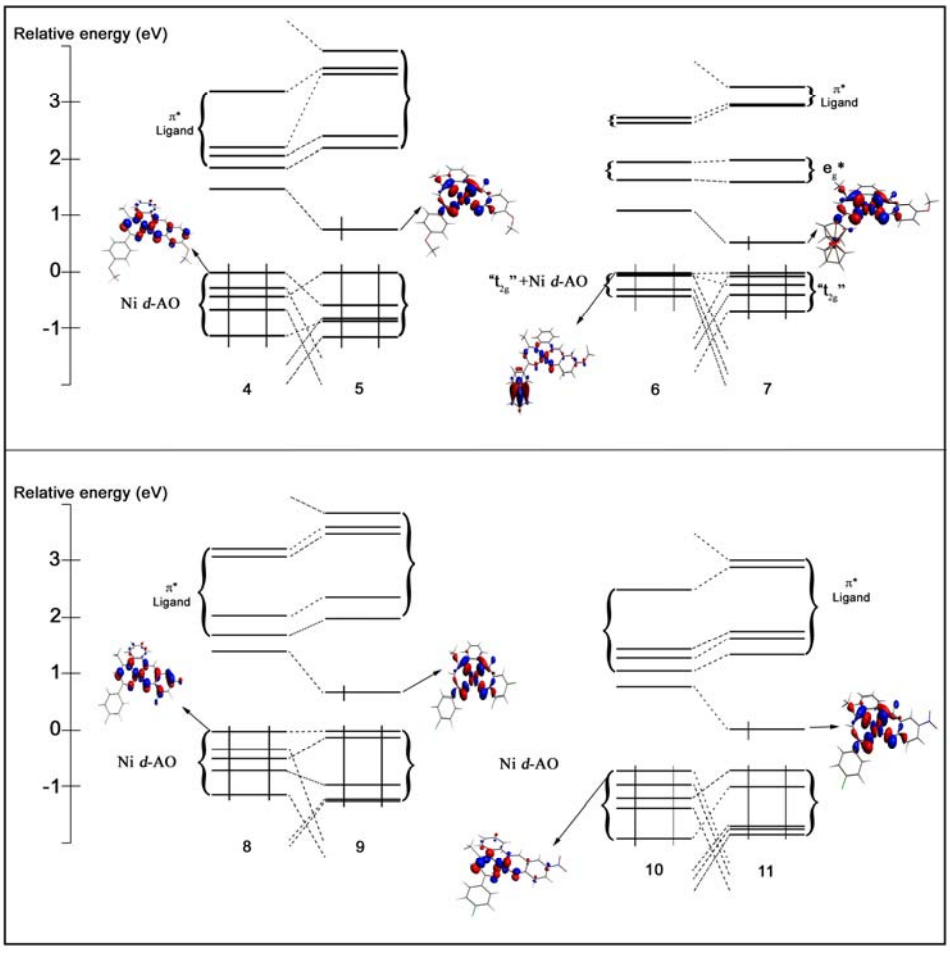

Fig. 8 MO diagrams of Ni(II) and Cu(II) complexes. For the sake of graphical simplicity and comparison, the diagrams of the Cu(II) species correspond to spin-restricted calculations.The HOMO energies have been arbitrarily set to zero for comparative purpose.

In the case of the Cu(II) compounds, the SOMO can be described as an antibonding combination of the Cu $d_{x^2-y^2}$ orbital with the proper combination of the ligand lone pairs (See Figs. 8 and S9-S16). The SOMOs have more metal than ligand character with a contribution around 46% of the $d_{x^2-y^2}$ orbital of the copper and around 37% of ligand orbitals. This is a typical situation for a d^9 Cu(II) square-planar complex [53,63]. These features agree with the monoelectronic reversible processes observed in the cathodic area of the CVs (see Section 3.6).

The spin density plots of the four Cu(II) complexes are shown in Fig. 9. Consistent with the significant ligand character of their SOMO, the computed Cu spin density is of 0.458, 0.456, 0.459 and 0.457, respectively. Their other frontier orbitals are the same as those of their Ni(II) homologues.

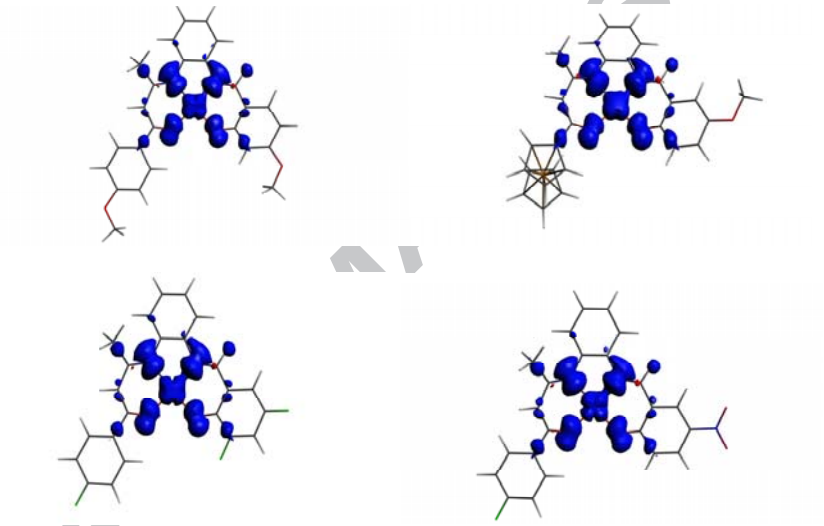

Fig. 9 Spin density plots of Cu(II) compounds **5**, **7**, **9** and **11**

Mulliken atomic charge calculations show that Cu(II) has a greater positive charge (~ +0.60) in **5**, **7**, **9** and **11**,than Ni(II) (~ +0.45) in **4**, **6**, **8** and **10** (Table 6). In the case of **6**, the charge density of Fe(II) is equal to -0.03, characterizing the electron releasing ability of the ferrrocenyl fragment, Accounting for its contribution to the MO and cyclic voltammetry response.

Finally, we complemented our theoretical investigation by analyzing the electronic spectra of the closed-shell d^8 Ni(II) complexes **4**, **6**, **8** and **10** through Time-Dependent Density Functional Theory (TD-DFT) calculations (see Section 2.7 for computational details). The simulated spectra (solvent effect not considered) are plotted on Fig. 10 together with the experimental ones. The main features of the experimental spectra are satisfactorily reproduced.

To analyze the theoretical spectra, the calculated transition with major oscillator strength was considered. This allowed to identify the main transition associated with calculated bands (Table 7). The high-energy bands are associated to ILCT π→π* type transition and Fc→ π*, transition in the case of compound **6**. The low-energy bands originated mainly from MLCT Ni→π* type transition and to a lesser extent from LMCT π → Ni type transition.

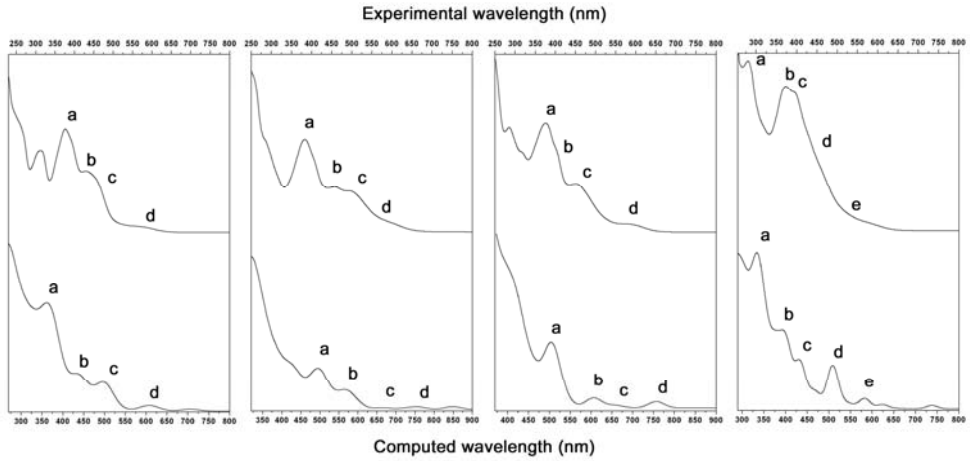

Fig. 10 Experimental (top) and computed (bottom) electronic absorption spectra of the Ni(II) complexes **4**, **6**, **8** and **10**

Table 7. Relevant transition assignments for Ni(II) complexes.

Comp.	Band	Assignments
4	A	ILCT π→π*
	B	MLCT Ni→π*
	C	MLCT Ni→π*
	D	LMCT π →Ni
6	A	MLCT Fc(t_2g) →π*
	B	ILCT π→π*
	C	MLCT Ni→π*
	D	LMCT π →Ni
8	A	ILCT π→π*
	B	MLCT Ni→π*
	C	MLCT Ni→π*
	D	LMCT π→Ni
10	A	ILCT π→π*
	B	MLCT Ni→π*
	C	MLCT Ni→π*
	D	LMCT π→Ni
	E	*d-d* Ni→Ni

4. Conclusions

In this study we offer the report of a series of unsymmetrically-substituted Ni(II) and Cu(II) complexes supported by two families of electron-releasing and electron-withdrawing N_2O_2-tetradentate Schiff base ligands. In the two D-π-D and A-π-A classes of compounds, the two donor or acceptor groups are connected through the conjugated M(II)-centered macroacyclic Schiff base core. They are easily synthetized via condensation reaction of appropriately substituted ONN-tridentate half-units and salicylaldehydes in the presence of a metal(II) salt. The eight complexes **4**-**11** were fully characterized and their electrochemical properties investigated. Single crystal X-ray diffraction analyses showed distorted square planar geometry of the M(N_2O_2) cores (M = Ni: **4**, Cu: **5**, **7**, **9** and **11**) inserted into a bowed unsymmetrically-substituted Schiff base scaffold, and revealed the partial delocalization of bonding electron density throughout the metal Schiff base skeleton. The solvated complexes **4**, **5**, **7** and **9** show hydrogen bond interactions between the crystallization solvent and the phenoxo oxygen atom of the macroacyclic Schiff base ligand. The unsolvated derivative **11** packs as a dimer in which the monomeric units are connected by apical Cu-O short-contact interactions leading to pentacoordinated Cu(II) centers with a square pyramidal coordination sphere. For all the complexes, geometry and electronic structure were analyzed using DFT and TD-DFT calculations. Overall these mono- and binuclear Ni and Cu complexes have the potential to serve as functional building blocks in the construction of extended D-π-A type compounds, and current efforts are now focused along this line.

Acknowledgments

The authors thank Prof. J.-Y. Saillard (ISCR, Rennes) for pertinent advices concerning the theoretical work, and Drs F. Lambert and P. Jehan (CRMPO, Rennes) for helpful assistance with HRMS. This research has been performed as part of the Chilean-French International Associated Laboratory for ‘’Inorganic Functional Materials’’ (LIAMIF-CNRS N°836). Financial support from the Fondo Nacional de Desarrollo Científico y Tecnológico [FONDECYT (Chile), grant no. 1130105 (D.C., C.M. and M.F.), the Vicerrectoría de Investigación y Estudios Avanzados, Pontificia Universidad Católica de Valparaíso, Chile (D.C., C.M. and M.F.), the CNRS and the Université de Rennes 1 is gratefully acknowledged. FEDER funds are also acknowledged for their participation in the purchase of the D8

VENTURE Bruker AXS diffractometer. J. C. thanks the CONICYT (Chile) for support of a graduate fellowship.

Appendix A. Supplementary material

CCDC 1523765-1523769 and 1523343 contain the supplementary crystallographic data for this paper. These data can be obtained free of charge from the Cambridge Crystallographic Data Centre via www.ccdc.cam.as.uk/data_request/cif.

Appendix B. Supplementary material

FT-IR, ^{1}H and ^{13}C NMR spectra and mass spectra (Figs. S1-S8), packing diagrams of **4**, **5**, **7**, **9** and **11** (Figs. S9-S13), UV-Vis spectra of **4**-**11** (Fig. S14), cyclic voltammograms of **4**-**11** (Figs. S15,S16), Molecular Orbitals diagrams of **4**-**11** (Figs. S17-S24) selected bond distances and angles for **4**, **5**, **7**, **9** and **11** (Tables S1-S3), hydrogen bonds in **4**, **5**, **7** and **9** (Table S4), computed bond distances and angles for **6**, **8** and **10** (Tables S5-S7), and Cartesian coordinates of all the optimized structures (Tables S8-S15).

References

[1] (a) M. Calligaris, L. Randaccio, in: G. Wilkinson, R.D. Gillard, J.A. McCleverty (Ed.), Comprehensive Coordination Chemistry, Pergamon Press, Oxford, 1987, pp. 715; (b) Y.-G. Li, D.-H. Shi, H.-L. Zhu, H. Yan, S.W. Ng, Inorg. Chim. Acta 360 (2007) 2881; (c) I. Rousso, N. Friedman, M. Sheves, M. Ottolenghi, Biochemistry 34 (1995) 12059; (d) T. Baasov, M. Sheves, Biochemistry 25 (1986) 5249 ; (e) R.D. Jones, D.A. Summerville, F. Basolo, Chem. Rev. 79 (1979) 139; (f) D.M. Kurtz Jr., D.W. Shriver, I.M. Klotz, Coord. Chem. Rev. 24 (1977) 145.

[2] (a) R. Hernandez-Molina, A. Mederos, in: J.A. McCleverty, T.J. Meyer (Eds.), Comprehensive Coordination Chemistry II, Elsevier Pergamon, Oxford, 2004, vol. 1, pp. 411; (b) A. Garcia-Deibe, A. Sousa, M.R. Bermejo, P.P. Mac Rory, C.A. McAuliffe, R.G. Pritchard, M. Helliwell, J. Chem. Soc. Chem. Commun. (1991) 728; (c) R. Atkins, G. Brewer, E. Kokot, G.M. Mockler, E. Sinn, Inorg. Chem. 24 (1985) 127; (d) P.G. Cozzi, Chem. Soc. Rev. 33 (2004) 410; (e) K.C. Gupta, A.K. Sutar, Coord. Chem. Rev. 252 (2008) 1420; (f) A.M. Abu-Dief, I.M.A. Mohamed, J. Basic Appl. Sci. 4 (2015) 119.

[3] Selected recent articles: (a) E.L. Gavey, M. Pilkington, Coord. Chem. Rev. 296 (2015) 125; (b) C.E. Satheesh, P. Raghavendra Kumar, P. Sharma, K. Lingaraju, B.S. Palakshamurthy, H. Raja Naika, Inorg. Chim. Acta 442 (2016) 1; (c) I. Sheikhshoaie, S.Y. Ebrahimipour, N. Lotfi, J.T. Mague, M. Khaleghi, Inorg. Chim. Acta 442 (2016) 151; (d) M. Salehi, F. Rahimifar, M. Kubicki, A. Asadi, Inorg. Chim. Acta 443 (2016) 28; (e) A. Kanti Ghosh, M. Mitra, A. Fathima, H. Yadav, A. Roy Choudhury, B. Unni Nair, R. Ghosh, Polyhedron 107 (2016) 1; (f) N. Mahlooji, M. Behzad, H. Amiri Rudbari, G. Bruno, B. Ghanbari, Inorg. Chim. Acta 445 (2016) 124; (g) L. Habala, S. Varényi, A. Bilková, P. Herich, J. Valentová, J. Kožíšek, F. Devínsky, Molecules 21 (2016) 1742; (h) H. Keypour, A. Shooshtari, M. Rezaeivala, F. Ozturk Kup, H. Amiri Rudbari, Polyhedron 97 (2015) 75; (i) S. Meghdadi, M. Amirnasr, M. Majedi, M. Bagheri, A. Amiri, S. Abbasi, K. Mereiter, Inorg. Chim. Acta 437 (2015) 64; (j) S.Y. Ebrahimipour, I. Sheikhshoaie, A.C. Kautz, M. Ameri, H. Pasban-Aliabadi, H.A. Rudbari, G. Bruno, C. Janiak, Polyhedron 93 (2015) 99; (k) T. Todorovic, S. Grubišic, M. Pregelj, M. Jagodic, S. Misirlic-Dencic, M. Dulovic, I. Olivera Klisuric, A. Maleševic, D. Mitic, K. Ancelkovic, N. Filipovic, Eur. J. Inorg. Chem. (2015) 3921.

[4] (a) H. Miyasaka, A. Saitoh, S. Abe, Coord. Chem. Rev. 251 (2007) 2622 ; (b) D. Venegas-Yazigi, D. Aravena, E. Spodine, E. Ruiz, S. Alvarez, Coord. Chem. Rev. 254 (2010) 2086; (c) N. Novoa, F. Justaud, P. Hamon, T. Roisnel, O. Cador, B. Le Guennic, C. Manzur, D. Carrillo, J.-R. Hamon, Polyhedron 86 (2015) 81; (d) J.P. Costes, S. Titos-Padilla, I. Oyarzabal, T. Gupta, C. Duhayon, G. Rajaraman, E. Colacio,Inorg. Chem. 55 (2016) 4428.

[5] (a) P. G. Lacroix, I. Malfant, C. Lepetit, Coord. Chem. Rev. 308 (2016,) 381; (b) C.R. Nayar, R. Ravikumar, J. Coord. Chem. 67 (2014) 1; (c) P.G. Lacroix, Eur. J. Inorg. Chem. (2001) 339; (d) S. di Bella, Chem. Soc. Rev. 30 (2001) 355.

[6] (a) L. Rigamonti, F. Demartin, A. Forni, S. Righetto, A. Pasini, Inorg. Chem. 45 (2006) 10976; (b) J. Gradinaru, A. Forni, V. Druta, F. Tessore, S. Zecchin, S. Quici, N. Garbalau, Inorg. Chem. 46 (2007) 884.

[7] Selected review articles and references therein: (a) P. Das, W. Linert, Coord. Chem. Rev. 311 (2016) 1; (b) C.-L. Ho, W.-Y. Wong, Coord. Chem. Rev. 255 (2011) 2469; (c) R.M. Haak, S.J. Wezenberg, A.W. Kleij, Chem. Commun. 46 (2010) 2713; (d) D.J. Darensbourg, Chem. Rev. 107 (2007) 2388; (e) K. Matsumoto, B. Saito, T. Katsuki, Chem. Commun. (2007) 3619; (f) C. Baleizo, H. Garcia, Chem. Rev. 106 (2006) 3987; (g) E.M. McGiarrigle, D.G. Gilheany, Chem. Rev. 105 (2005) 1563; (h) E.N. Jacobsen, Acc. Chem. Res. 33 (2000) 421; (i) L. Canali, D.C. Sherrington, Chem. Soc. Rev. 28 (1999) 85.

[8] For very recent articles, see for example: (a) H.-W. Ou, K.-H. Lo, W.-T. Du, W.-Y. Lu, W.-J. Chuang, B.-H. Huang, H.-Y. Chen, C.-C. Lin, Inorg. Chem. 55 (2016) 1423; (b) H.-C. Tseng, H.-Y. Chen, Y.-T. Huang, W.-Y. Lu, Y.-L. Chang, M. Y. Chiang, Y.-C. Lai, H.-Y. Chen, Inorg. Chem. 55 (2016) 1642; (c) W.-G. Jia, H. Zhang, T. Zhang, D. Xie, S. Ling, E.-H. Sheng, Organometallics 35 (2016) 503; (d) C.W. Anson, S. Ghosh, S. Hammes-Schiffer, S.S. Stahl, J. Am. Chem. Soc. 138 (2016) 4186; (e) X.-P. Zeng, Z.-Y. Cao, X. Wang, L. Chen, F. Zhou, F. Zhu, C.-H. Wang, J. Zhou, J. Am. Chem. Soc. 138 (2016) 416, (f) S. Menati, H. Amiri Rudbari, B. Askari, M. Riahi Farsani, F. Jalilian, G. Dini, C. R. Chimie 19 (2016) 347.

[9] (a) P. Guerriero, S. Tarnburini, P.A. Vigato, Coord. Chem. Rev. 139 (1995,) 17; (b) N.E. Borisova, M.D. Reshetova, Y.A. Ustynyuk, Chem. Rev. 107 (2007) 46; (c) F.Y. Wei, Russ. J. Coord. Chem. 42 (2016) 44.

[10] A.W. Kleij, Eur. J. Inorg. Chem. (2009) 193.

[11] J.P. Costes, F.Z. Chiboub Fellah, F. Dahan, C. Duhayon, Polyhedron 52 (2013) 1065.

[12] (a) J.P. Costes, Polyhedron 6 (1987) 2169 and references cited therein; (b) E. Kwiatkowski, M. Kwiatkowski, Inorg. Chim. Acta 82 (1984) 101; (c) G. Bett, D.E. Fenton, J.R. Tate, Inorg. Chim. Acta 54 (1981) L101.

[13] (a) A. Trujillo, M. Fuentealba, D. Carrillo, C. Manzur, I. Ledoux-Rak, J.-R. Hamon, J.-Y. Saillard, Inorg. Chem. 49 (2010) 2750; (b) S. Celedón, M. Fuentealba, T. Roisnel, I. Ledoux-Rak, J.-R. Hamon, D. Carrillo, C. Manzur, Eur. J. Inorg. Chem. (2016) 3012.

[14] (a) A.W. Kleij, D.M. Tooke, A.L. Spek, J.N.H. Reek, Eur. J. Inorg. Chem. (2005) 4626; (b) A. Dalla Cort, L. Mandolini, G. Palmieri, C. Pasquini, L. Schiaffino, Chem. Commun. (2003) 2178; (c) J. Lopez, S. Liang, X.R. Bu, Tetrahedron Lett. 39 (1998) 4199; (d) J. Lopez, E.A. Mintz, F.-L. Hsu, X.R. Bu, Tetrahedron: Asym. 9 (1998) 3741.

[15] (a) J.P. Costes, Bull. Soc. Chim. Fr. (1986) 78; (b) S.K. Mandal, K. Nag, J. Chem. Soc. Dalton Trans. (1984) 2839.

[16] (a) G. Cros, J.P. Costes, C. R. Acad. Sci. Paris, 294 (1982) 173; (b) J.P. Costes, G. Cros, M.H. Darbieu, J.-P. Laurent, Inorg. Chim. Acta 60 (1982) 111; (c) J.P. Costes, F. Dahan, J.-P. Laurent, J. Coord. Chem. 13 (1984) 355.

[17] (a) S. Chattopadhyay, M. Sinha, S. Chaudhuri, Inorg. Chim. Acta 359 (2006) 1367; (b) M.S. Ray, R. Bhattacharya, S. Chaudhuri, L. Righi, G. Bocelli, G. Mukhopadhyay, A. Ghosh, Polyhedron 22 (2003) 617; (c) A. Garcia-Deibe, M.R. Bermejo, A. Sousa, C.A. Mcauli.e, P. McGlyur, P.T. Ndifon, R.G. Pritchard, J. Chem. Soc., Dalton Trans. (1993) 1605; (d) N. Matsumoto, T. Akui, H. Murakami, J. Kanesaka, A. Ohyoshi, H. kawa, J. Chem. Soc. Dalton Trans. (1988) 1021; (e) J.P. Costes, Inorg. Chim. Acta 130 (1987) 17.

[18] B. Sarkar, G. Bocelli, A. Cantoni, A. Ghosh, Polyhedron 27 (2008) 693.

[19] B. Sarkar, M.S. Ray, M.G.B. Drew, A. Figuerola, C. Diaz, A. Ghosh, Polyhedron 25 (2006) 3084.

[20] A. Trujillo, S. Sinbandhit, L. Toupet, D. Carrillo, C. Manzur, J.-R. Hamon, J. Inorg. Organomet. Polym. Mater. 18 (2008) 81.

[21] P. Hu, L. Zhang, X. Zhu, X. Liu, L. Ji, Y. Chen, Polyhedron 8 (1989) 2459.

[22] S. Celedon, M. Fuentealba, T. Roisnel, J.-R. Hamon, D. Carrillo, C. Manzur, Inorg. Chim. Acta 390 (2012) 184.

[23] M. Fuentealba, A. Trujillo, J.-R. Hamon, D. Carrillo, C. Manzur, J. Mol. Struct. 881 (2008) 76.

[24] (a) M. Fuentealba, J.-R. Hamon, D. Carrillo, C. Manzur, New J. Chem. 31 (2007) 1815; (b) A. Trujillo, M. Fuentealba, D. Carrillo, C. Manzur, J.-R. Hamon, J. Organomet. Chem. 694 (2009) 1435; (c) A. Trujillo, F. Justaud, L. Toupet, O. Cador, D. Carrillo, C. Manzur, J.-R. Hamon, New J. Chem. 35 (2011) 2027; (d) N. Novoa, J. P. Soto, R. Henríquez, C. Manzur, D. Carrillo, J.-R. Hamon, J. Inorg. Organomet. Polym. Mater. 23 (2013) 1247.

[25] (a) S. Celedón, V. Dorcet, T. Roisnel, A. Singh, I. Ledoux-Rak, J.-R. Hamon, D. Carrillo, C. Manzur, Eur. J. Inorg. Chem. (2014) 4984; (b) J. Cisterna, V. Dorcet, C. Manzur, I. Ledoux-Rak, J.-R. Hamon, D. Carrillo, Inorg. Chim. Acta 430 (2015) 82.

[26] W.L.F. Armarego, C.L.L. Chai, Purification of Laboratory Chemicals, Fifth ed., Butterworth-Heinemann, Elsevier Inc., Amsterdam, The Netherlands, 2003.

[27] V.V. Popic, S.M.; Korneev, V.A. Nikolaev, I.K. Korobitsyna, Synthesis (1991) 195.

[28] X. Shen, A. Jyoti Borah, X. Cao, W. Pan, G. Yan, X. Wu, Tetrahedron Lett. 56 (2015) 6484.

[29] APEX2, Bruker AXS Inc., Madison, Wisconsin, USA,. 2007.

[30] O.V. Dolomanov, L.J. Bourhis, R.J. Gildea, J.A.K. Howard, H. Puschmann, J. Appl. Crystallogr. 42 (2009) 339.

[31] G.M. Sheldrick, Acta Crystallogr. A64 (2008) 112.

[32] L.J. Bourhis, O.V. Dolomanov, R.J. Gildea, J.a.K. Howard, H. Puschmann, Acta Crystallogr. A71 (2015) 59.

[33] A. Altomare, M.C. Burla, M. Camalli, G. Cascarano, C. Giacovazzo, A. Guagliardi, A.G.G. Moliterni, G. Polidori, R. Spagna, J. Appl. Crystallogr. 32 (1999) 115.

[34] G.M. Sheldrick, Acta Crystallogr. C71 (2015) 3.

[35] E.J. Baerends, D.E. Ellis, P. Ros, Chem. Phys. 2 (1973) 41.

[36] P.M. Boerrigter, G. Te Velde, E.J. Baerends, Int. J. Quantum Chem. 33 (1988) 87.

[37] G. Te Velde, E.J. Baerends, J. Comput. Phys. 99 (1992) 84.

[38] C. Adamo, D. Jacquemin, Chem. Soc. Rev. 42 (2013) 845.

[39] Y.J. Bomble, J. Am. Chem. Soc. 128 (2006) 3103.

[40] G. Te Velde, F.M. Bickelhaupt, E.J. Baerends, C. Fonseca Guerra, S.J.A. van Gisbergen, J.G. Snijders, T. Ziegler, J. Comput. Chem. 22 (2001) 931.

[41] S.H. Vosko, L. Wilk, M. Nusair, Can. J. Phys. 58 (1980) 1200.

[42] A.D. Becke, J. Chem. Phys. 84 (1986) 4524.

[43] A.D. Becke, Phys. Rev. A38 (1988) 3098.

[44] J. Perdew, Phys. Rev. B 33 (1986) 8822.

[45] J. Perdew, Phys. Rev. B 34 (1986) 7406.

[46] L. Versluis, T. Ziegler, J. Chem. Phys. 88 (1988) 322.

[47] S.J.A. Van Gisbergen, J.G. Snijders, E.J. Baerends, Comput. Phys. Commun. 118 (1999) 119.

[48] A.D. Becke, J. Chem. Phys. 98 (1993) 5648.

[49] J. Tirado-Rives, W.L. Jorgensen, J. Chem. Theory Comput. 4 (2008) 297.

[50] (a) C. Gallardo, A. Trujillo, M. Fuentealba, A. Vega, D. Carrillo, C. Manzur, J. Chil. Chem. Soc. 52 (2007) 1266; (b) D. Lloyd, D.R. Marshall, J. Chem. Soc. (1956) 2597.

[51] D. Lin-Vien, N.B. Colthup, W.G. Fateley, J.G. Grasselli, Handbook of Infrared and Raman Characteristic Frequencies of Organic Molecules, Elsevier, 1991. See: (a) Ch. 10, pp. 155-178; (b) Ch. 3, pp. 29-44; (c) Ch. 17, pp. 277-306; (d) Ch. 11, pp. 179-189.

[52] (a) M.A. Gaona, F. Montilla, E. Álvarez, A. Galindo, Dalton Trans. 44 (2015) 6516; (b) J.V. Greenhill, Chem. Soc. Rev. 6 (1977) 277.

[53] N. Novoa, T. Roisnel, P. Hamon, S. Kahlal, C. Manzur, H. M. Ngo, I. Ledoux-Rak, J.-Y. Saillard, D. Carrillo, J.-R. Hamon, Dalton Trans. 44 (2015) 18019.

[54] (a) S. Sharif, G.S. Denisov, M.D. Toney, H.-H. Limbach, J. Am. Chem. Soc. 128 (2006) 3375; (b) T. Dziembowska, M. Szafran, A. Katrusiak, Z. Rozwadowski, J. Mol. Struct. 929 (2009) 32; (c) B. Kukawska-Tarnawska, A. Le?, T. Dziembowska, Z.J. Rozwadowski, J. Mol. Struct. 928 (2009) 25; (d) A. Ba?o?lu, S. Parlayan, M. Ocak, H. Alp, H. Kantekin, M. Özdemir, Ü. Ocak, Polyhedron 28 (2009) 1115.

[55] N. Novoa, T. Roisnel, V. Dorcet, O. Cador, C. Manzur, D. Carrillo, J.-R. Hamon, New J. Chem. 40 (2016) 5920.

[56] G.R. Desiraju, T. Steiner, The Weak Hydrogen Bond, Oxford University Press Inc., New York, 1999.

[57] (a) G. J. Long, P. J. Clarke, Inorg. Chem. 17 (1978) 1395; (b) R.E. Bachman, K.H. Whitemire, S.Mandal,P.K. Bharadwaj, Acta Crystallogr. C48 (1992) 1836.

[58] H. Zhang, L. Fang, Acta Crystallogr. E61 (2005) m180.

[59] a) E. Pereira, L. Gomes, B. de Castro, Inorg. Chim. Acta 271 (1998) 83; (b) a. Anthonysamy, S. Balasubramanian, Inorg. Chem. Commun. 8 (2005) 908; (c) A.H. Kianfar, L. Keramat, M. Dostani, M. Shamsipur, M. Roushani, F. Nikpour, Spectrochim. Acta Part A Mol. Biomol. Spectrosc. 77 (2010) 424.

[60] (a) S. Zolezzi, E. Spodine, A. Decinti, Polyhedron 21 (2002) 55; (b) S. Gupta, S. Pal, A.K. Barik, A. Hazra, S. Roy, T.N. Mandal, S.-M. Peng, G.-H. Lee, M. Salah El Fallah, J. Tercero, S.K. Kar, Polyhedron 27 (2008) 2519; (c) A. Biswas, M.G.B. Drew, A. Ghosh, Polyhedron 29 (2010) 1029.

[61] P. Zanello, in Ferrocenes, A. Togni and T. Hayashi, Eds., VCH, New York, 1995; Chapter 7, pp. 317-430.

[62] D. Astruc, Electron Transfer and Radical Reactions in Transition-Metal Chemistry, VCH: New York, 1995, Chapter 2, Electrochemistry, pp. 89.

[63] M. Fuentealba, M.T. Garland, D. Carrillo, C. Manzur, J.-R. Hamon, J.-Y. Saillard, Dalton Trans. (2008) 77.

[64] T.A. Albright, J.K. Burdett, M.H. Whangbo,: Orbitals Interactions in Chemistry, Wiley, New York, 1985.

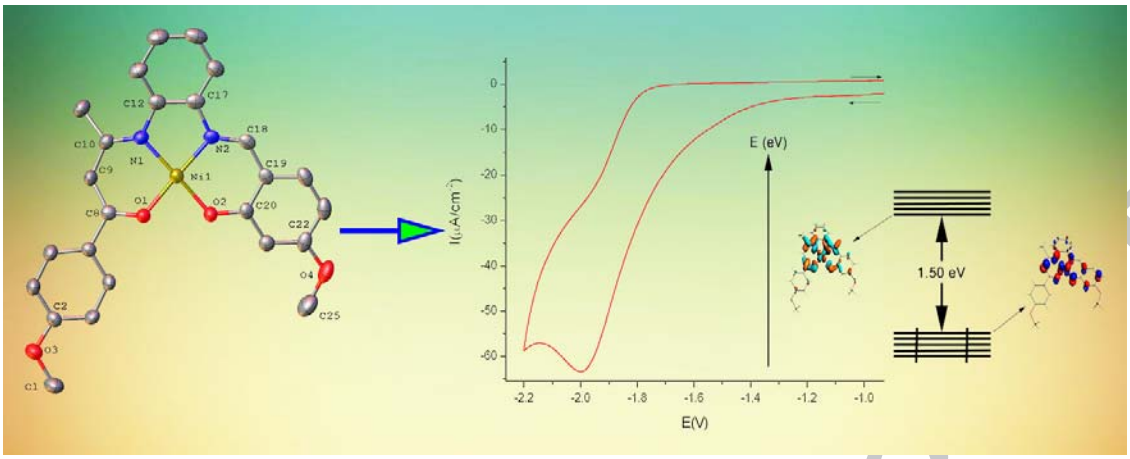

Two series of robust neutral Nickel(II)-and Copper(II) complexes supported by asymmetrical N2O2-tetradentate Schiff base ligands substituted by either a pair of electron releasing or electron withdrawing groups, forming D-π-D or A-π-A systems, respectively, have been investigated and their electronic structures analyzed by DFT and TD-DFT calculations.

binuclear push-pull unsymmetrical Schiff base complexes were synthesized and fully characterized. Those D-π-A conjugated systems that are all redox active and exhibit high thermal stability and good second-order NLO responses, contain a ferrocene donor linked to acceptor 5-NO_2 or 3,5-F_2 substituted salicylidene through a central M(N2O2) core (M = Ni, Cu).

HIGHLIGHTS

- Templated synthesis of D-π-D and A-π-A Ni(II)-and Cu(II)-N_2O_2 Schiff base complexes
- Anisyl, ferrocenyl and methoxy as donors, fluoro and nitro as acceptors
- Characterization by elemental analysis, absorption and multinuclear NMR spectroscopy
- X-ray crystal structure of one Ni and two Cu D-π-D derivatives
- X-ray crystal structure of two A-π-A Cu derivatives
- Optimized geometries and electronic structures analysed by DFT and TDDFT calculation